

1 Parameterization of particle formation rates in distinct atmospheric environments

2 Xinyang Li^{1,*}, Tuomo Nieminen^{1,2}, Rima Baalbaki^{1,3}, Putian Zhou¹, Pauli Paasonen¹, Risto Makkonen⁴, Martha A.
3 Zaidan^{1,5}, Nina Sarnela¹, Chao Yan^{1,6}, Tuija Jokinen^{1,3}, Imre Salma⁷, Máté Vörösmarty⁸, Tuukka Petäjä¹, Veli-Matti
4 Kerminen¹, Markku Kulmala^{1,6}, Lubna Dada^{1,9,*}

5 ¹ Institute for Atmospheric and Earth System Research (INAR), University of Helsinki, Helsinki, 00560, Finland

6 ² Department of Physics, Faculty of Science, University of Helsinki, Helsinki, Finland

7 ³ Climate & Atmosphere Research Centre (CARE-C), Cyprus Institute, P.O. Box 27456, Nicosia, 1645, Cyprus

8 ⁴ Hevesy Climate System Research, Finnish Meteorological Institute, P.O. Box 503, 00101 Helsinki, Finland

9 ⁵ Department of Computer Science, University of Helsinki, Helsinki, 00560, Finland

10 ⁶ Joint International Research Laboratory of Atmospheric and Earth System Sciences, School of Atmospheric Sciences, Nanjing University,
11 Nanjing, 210023, China

12 ⁷ Institute of Chemistry, Eötvös Loránd University, Budapest, Hungary

13 ⁸ Hevesy György Ph.D. School of Chemistry, Eötvös Loránd University, Budapest, Hungary

14 ⁹ PSI Center for Energy and Environmental Sciences, Villigen PSI, Switzerland

15 *Correspondence to: Xinyang Li (xinyang.li@helsinki.fi), Lubna Dada (lubna.dada@helsinki.fi)

16

17 **Abstract.** Atmospheric particle formation rate (J) is one of the key characteristics in new particle formation (NPF)
18 processes worldwide. It is related to the development of ultrafine particle growth to cloud condensation nuclei
19 (CCN) and, hence, to Earth radiative forcing in global models, which helps us to better understand the impact of
20 NPF on cloud properties and climate change. In this work, we parameterized four semi-empirical J models for 5
21 nm atmospheric particles using field measurements obtained from distinct environments that varied from clean to
22 heavily polluted regions and from tropical to polar regions. The models rely primarily on sulfuric acid as a
23 condensing vapor, condensation sink to account for the vapor loss, and relative humidity for meteorological
24 contribution to J . However, the dependencies between J , condensation sink, and relative humidity are affected by
25 their interlinked relations to sources and sinks of other condensable vapors than sulfuric acid and the potential
26 traffic emissions to the observed size range. The parameterization results showed that our models were able to
27 produce plausible predictions for boreal forest environments, heavily polluted environments, and biogenic
28 environments with high relative humidity. We further tested the models in the global simulation module Tracer
29 Model 5 (TM5, massive parallel version) to simulate particle number size distribution across 14 global atmospheric

measurement sites. The simulated results showed satisfactory predictions on particle number concentrations for all the tested environments, with significant improvement in the nucleation mode, and better prediction accuracy for Aitken and accumulation modes compared to the binary sulfuric acid-organic vapor model in Riccobono (2014). Our study has successfully provided powerful tools to predict J_5 on a global scale across various environment types using the most essential and more accessible variables involved in the NPF processes. Essentially, this work reinforces the necessity for global research into the investigation of environment-oriented meteorology-involved NPF processes.

1 Introduction

Atmospheric new particle formation (NPF) is a natural phenomenon observed globally (Bousiotis et al., 2021; Brean et al., 2023; Gordon et al., 2017; Kerminen et al., 2018; Nieminen et al., 2018). As particles form and grow on regional scales, they can reach large enough sizes at which they can act as cloud condensation nuclei (CCN) for water vapor to condense onto when forming clouds. This process affects cloud properties (Roldin et al., 2011; Sanchez et al., 2016; Spracklen et al., 2008) and ultimately the global climate depending on the particle numbers, sizes and their chemical compositions (Bellouin et al., 2020; Calvo et al., 2013; Uno et al., 2020). Particle formation rate (J) is an essential parameter describing the NPF intensity, which is often utilized to represent NPF in global models to simulate the effect of NPF on cloud properties and radiative forcing on Earth. To derive a representative parametrization of J for global simulation, we require a broad understanding of NPF in different environments temporally and spatially. That being the case, the atmospheric measurements of both particle number size distributions and NPF precursor vapors are essential to obtain for the atmospheric observations and model developments.

The NPF processes have been investigated and parameterized based on particle formation mechanism theories (Chang et al., 2009; Kulmala et al., 2001; Lehtinen and Kulmala, 2003), field measurements from specific environments, such as pristine boreal forests (Kulmala et al., 2001; Nieminen et al., 2011; Paasonen et al., 2010), urban cities (Salma et al., 2011, 2016, 2021; Salma and Németh, 2019; Zhang et al., 2010), rural area (Lee et al., 2019; Yli-Juuti et al., 2009), marine environment (Zhang et al., 2010), and also chamber experiments (Kirkby et al., 2011; Lehtipalo et al., 2018). In addition to neutral particle formation mechanisms, the ion-induced nucleation is also covered in J parameterizations (e.g. Nieminen et al., 2011; Määttänen et al., 2018). The existing literature primarily focused on the particle activation and survival of nucleation mode particles down to 1.5 nm, involving complex micro-physics of aerosol particles, such as nanometer clusters production, losses due to clusters

59 coagulation and growth (Bousiotis et al., 2021; Chu et al., 2019; Kerminen et al., 2018; Nieminen et al., 2018).
60 Furthermore, distinct effects on particle formation rates influenced by the same factors were seen under comparable
61 environmental settings. However, these environment-specific models typically have limited application for global
62 simulation implementations that encompass the diverse atmospheric conditions on Earth.

63 To simulate particle formation rates, one usually starts from the nucleation mode size range. Global modelers have
64 been facing great challenges in simulating nucleation mode particles because large-scale models have limited
65 capabilities in treating the complicated aerosol dynamics taking place in the sub-5 nm particle size range. The
66 formation rate at 5 nm is shown to be important because after sizes of about a few nm in diameter, particle growth
67 rates show relatively limited variability in different environments (Kulmala et al., 2022a, b, 2023). In addition, we
68 currently do not have a good enough theoretical understanding on the processes dictating particle growth rates at
69 the smallest sizes, nor the survival of such particles from coagulation scavenging (e.g. Cai et al., 2022; Tuovinen
70 et al., 2022; Marten et al., 2022).

71 The essential parameters for J parameterizations should include at least one type of precursor vapor, some may
72 also cover meteorological parameters, and the sinks for vapors and particles. For instance, sulfuric acid (H_2SO_4) as
73 the most known precursor vapor plays a critical role in particle formation and growth processes due to its low
74 volatility (Kulmala et al., 2004; Myllys et al., 2019). In the earlier parameterizations of NPF mechanism, J
75 correlated (linearly or squared) with H_2SO_4 concentrations in various environments (Paasonen et al., 2010). In
76 terms of meteorology, air temperature (T), relative humidity (RH), global solar radiation (GRad), wind speed (WS),
77 and wind direction influence the particle formation rates in certain environments as well (Laarne et al., 2022; Salma
78 et al., 2021; Zaidan et al., 2018). The variation of T can influence the precursor vapor formation and stability of
79 NPF processes: a higher T can enhance the biogenic emissions that participate in particle formation in a boreal
80 forest (Dada et al., 2017; Nieminen et al., 2015), while a lower T favored the H_2SO_4 -amine clusters stability in a
81 megacity (Deng et al., 2020). RH can impact the precursor vapor formations as well as the aerosol formation rates
82 (Ding et al., 2021; Hellmuth, 2006). The variation of RH is dependent upon T so that the rise of T during daytime
83 increases the planetary boundary layer height (PBLH), which in turn dilutes the air mixture and decreases the RH
84 (Liu et al., 2018) as well as particle number concentrations (Mazon et al., 2016) in the atmosphere. For condensable
85 vapor loss, we usually include the term condensation sink (CS), which describes the loss rate of condensable vapors
86 to aerosol particles, and it typically declines before an NPF event starts. H_2SO_4 concentrations, on the other hand,
87 increase due to the reduction in CS, which means that the condensable vapors are not lost onto the aerosol particles
88 as efficiently as they would be at greater CS values (Hellmuth, 2006; Kulmala et al., 2012).

89 In general, the developed J models underestimate the observed particle number concentration, which may be
90 attributed to NPF schemes being poorly represented in these models. Many J parameterization works were
91 conducted focusing on the formation mechanisms from sulfuric acid (Paasonen et al., 2010), sulfuric acid-water
92 (Määttänen et al., 2018), sulfuric acid-ammonia (Glasoe et al., 2015), and sulfuric acid-organic vapor (Paasonen et
93 al., 2010; Riccobono et al., 2014). However, some models are likely applicable only to certain types of environment,
94 or they primarily cover the microphysics of the particle nucleation at sub-3 nm range, where the nucleated clusters
95 face higher instability due to the higher evaporation rates than condensation rates (Deng et al., 2021; Wang et al.,
96 2011). Bergman (2022) attempted an organic-vapor-based NPF scheme in addition to the commonly used binary
97 water-sulfuric-acid-based scheme to simulate global particle formation and number concentrations. This scheme
98 improved the simulated number concentrations across the observation stations, although they were still
99 underestimated compared to the observations, suggesting that the parameterization of early growth of particles to
100 5 nm diameter still requires improvement.

101 To predict the particle formation rate at 5 nm originating from NPF and subsequent growth, as well as to understand
102 and predict the climatic impacts caused by NPF and initial growth in global scale, we parameterize particle
103 formation rates (J) at 5 nm using combined measurement data from six different environments: Hyytiälä (boreal
104 forest close to rural environment, Finland), Beijing (megacity, China), Värriö (remote boreal forest, Finland),
105 Budapest (urban, Hungary), Agia Marina Xyliatos (rural, Cyprus) and Manacapuru (Amazonian basin, Brazil). The
106 parameterizations of J were based on the analysis of atmospheric particle number-size distributions. Sulfuric acid
107 concentrations, RH and CS are the main input variables in the parameterization models. By including information
108 from various types of environments, we will be able to demonstrate whether our models can adequately explain the
109 formation rate of 5 nm particles on a wider environmental scale. The parameterized models are then incorporated
110 into EC-Earth models to simulate particle formation rates in the global scale (the European community Earth-
111 System Model, EC-Earth, chemistry transport model TM5: Tracer Model 5, version TM5-chem-v3.0, details in
112 supplement) (Huijnen et al., 2010).

113 This work aims to provide an effective tool for global particle formation rate estimations. Our parameterizations
114 have three main features: (1) the number of inputs is limited to be the most essential parameters involved in NPF
115 process, (2) they do not involve complex microphysics at particles smaller than 5 nm, and (3) they cover a wide
116 range of environment types. These features will enhance the applicability of the parameterizations for the purpose
117 of global model application.

118 **2 Measurement locations and instrumentation**

119 This study includes measurements from six different sites representing different environmental conditions. A
120 summary for all locations and the instrumentation used is given in Table S1. Figure 1 shows the map of the
121 measurement sites included in this study.

122 **2.1 Measurement sites**

123 **2.1.1 Rural boreal forest environment: Hyytiälä, Finland**

124 The measurement data were obtained from the SMEAR II-station (Station for Measuring Ecosystem–Atmosphere
125 Relations), situated in a Scots pine (*Pinus sylvestris*) forest in Hyytiälä (61.1° N, 24.17° E; 181 m (a.s.l.); Hari and
126 Kulmala, 2005), southern Finland. This measurement site is described as having a rural regional background with
127 minimal anthropogenic emission. Hyytiälä data covered the period from 21 March 2016 to 18 August 2019.

128 **2.1.2 Remote sub-arctic boreal forest: Värriö, Finland**

129 The SMEAR I measurement station (67°45′31″ N, 29°36′41″ E, 390 m a.s.l.) was built on the top of Kotovaara hill
130 located in north-eastern Finland. Similar to Hyytiälä, the site is also a rural background covered mainly by Scots
131 pine (*Pinus sylvestris*) forest located at the north side of the Värriö fell range. However, it is affected by potential
132 polluted air mass that comes from Kola peninsula rather than local industrial pollutants. A detailed description of
133 SMEAR I station can be found in (Kyrö et al., 2014). The data used from Värriö were from 5 April to 13 August
134 2019.

135 **2.1.3 Polluted megacity: Beijing, China**

136 In Beijing, the measurements were performed at the west campus of the Beijing University of Chemical Technology
137 (BUCT, 39.94° N, 116.30° E, 20 m a.s.l.). The sampling took place from outside the window on the 5th floor of the
138 university building close to a street with busy traffic. For more details on the description of BUCT measurement
139 site, see Liu et al., 2020. The data were available from 29 May 2018 to 3 April 2019.

140 **2.1.4 Urban site: Budapest, Hungary**

141 The measurements took place at the Budapest platform for Aerosol Research and Training (BpART) Laboratory
142 (47.47° N, 19.06° E; 115 m a.s.l.) of the Eötvös Loránd University situated on the bank of the river Danube. The
143 site represents a mixed average atmosphere of the city center (Salma et al., 2016). The data were obtained from 22
144 March to 17 April 2018.

145 **2.1.5 Mediterranean rural site: Agia Marina, Cyprus**

146 The measurements were conducted at the Agia Marina Xyliatou (AMX) station (35.03° N, 33.05° E; 532 m a.s.l.)
147 of the Cyprus Atmospheric Observatory (CAO). The site represents a rural background location situated at the
148 foothills of Troodos mountains, with agriculture land in the vicinity. The data were obtained between 22 February
149 and 3 March 2018. For more details about the site, see e.g. Baalbaki et al., (2021).

150 **2.1.6 Amazonian basin: Manacapuru, Brazil**

151 The Manacapuru measurement site was in a pastureland 70 km west of Manaus, Brazil, in central Amazonia. This
152 site receives air mass from various resources, including rural, biogenic and anthropogenic from the nearby
153 municipality (Manaus). The trace gases and meteorological measurements were performed during the
154 GoAmazon2014/5 campaign at the T3 site (3.2133° S, 60.5987° W 50 m a.s.l.), 10 km northeast of Manacapuru,
155 Brazil (Martin et al., 2016; Schiro et al., 2018). A more detailed description of the measurement site can be found
156 in (Myers et al., 2022). The data covered the time period from 22 August 2014 to 9 October 2014.

157 **2.2 Instrumentation**

158 **2.2.1 Sulfuric acid measurements and proxies**

159 H₂SO₄ concentrations were measured at all sites, except for the Amazonian basin, using a Chemical Ionization
160 Atmospheric Pressure interface Time-of-Flight spectrometer (CI-APi-ToF) (Eisele and Tanner, 1993; Jokinen et
161 al., 2012) with NO₃⁻ as the reagent ion and analyzed using tofTools package based on MATLAB software
162 (Junninen et al., 2010). In the Amazonian basin, H₂SO₄ concentrations were measured using a selected ion chemical
163 ionization mass spectrometer (SICIMS), see Myers et al., (2022) for more details. The H₂SO₄ concentration
164 measurements were taken from different levels ranging from ground level up to 35 meters above ground level. The
165 CI-APi-ToFs were calibrated uniformly before the measurement in each location following the technique described

166 by (Kürten et al., 2012), except for the Amazonian basin where the selected ion chemical ionization mass
167 spectrometer (SICIMS) was calibrated following the scheme described in Mauldin III et al. (1998).
168 To increase the applicability of our derived parameterization, H₂SO₄ proxy data from Hyytiälä and Beijing were
169 included as an additional testing data set. The proxy data were calculated using the proxy specific for the boreal
170 forest environment and polluted megacity developed by Dada et al., (2020). For Hyytiälä, the sulfuric acid proxy
171 data ranged from 22 August to 25 December 2016, and 8 March 2018 to 26 February 2019, denoted as Hyytiälä_{SAprx};
172 For Beijing, the time period was from 15 March to 3 April 2019, denoted as Beijing_{SAprx}. The subscript “SA_{prx}”
173 (SA as in sulfuric acid) in Hyytiälä_{SAprx} and Beijing_{SAprx} indicates that the datasets utilize H₂SO₄ concentration from
174 proxies as input for the testing dataset.

175 **2.2.2 Particle number size distribution**

176 The particle number size distribution (PNSD) measurements were obtained from different types of setups in each
177 site. Hyytiälä: twin-Differential Mobility Particle Sizers (DMPS; Aalto et al., 2001); Värriö: Differential Mobility
178 Particle Sizers (DMPS) (Jokinen et al., 2022); Beijing: Particle Size Distribution (PSD) system with a nano-
179 Differential Mobility Analyzer (DMA) and an Aerodynamic Particle Sizer (APS) (Zhou et al., 2021); Budapest:
180 flow-switching-type DMPS (6 – 1000 nm; Salma et al., 2016); Cyprus: Neutral cluster and Air Ion Spectrometer
181 (NAIS) and Scanning Mobility Particle Sizer (SMPS; Baalbaki et al., 2021); Amazonian basin: the measurements
182 were conducted using SMPS (10 – 1000 nm). It is important to note that we do not aim to compare the PNSD
183 measurements from all the chosen sites. Instead, the PNSD measurements were used to calculate the formation
184 rates based on changes in particle number concentrations under local conditions.

185 **2.2.3 Meteorological variable**

186 The meteorological variables included in this study are relative humidity (RH, %) and ambient temperature (T , °C).
187 In Hyytiälä, RH and T were measured at 16.8 m using Rotronic MP102H RH sensor (Rotronic Hygromet MP102H
188 with Hygroclip HC2–S3, Rotronic AG, Bassersdorf, Switzerland); In Värriö, RH and T were measured by a
189 Rotronic MP106A captive sensor; In Beijing, RH and T were monitored by Vaisala weather station (AWS310); In
190 Budapest, RH and T were monitored using Vaisala HMP45D temperature and humidity probe, and Vaisala
191 WAV15A anemometer located on on-site of the BpART Lab; In Cyprus, RH and T were measured by a
192 meteorological station in a nearby village (35.01° N, 33.05° E), 2.85 km away from the measurement site; In
193 Amazonian basin, RH and T were measured at the Atmospheric Radiation Measurement (ARM) user facility.

194 2.3 Data analysis

195 2.3.1 Calculation of particle formation rates

196 To develop more inclusive and generalized models, the parameterization included data from both NPF event days
197 and non-event days. This approach recognizes that the production of atmospheric secondary particles from non-
198 NPF events (days with no apparent particle growth) is becoming more significant in a world with growing
199 anthropogenic influence (Kulmala et al., 2022a). Such a measure would increase the applicability of our models on
200 a global scale.

201 The observed particle formation rates (J_5) at 5 nm were calculated from the measured PNSD according to Equation
202 1 (Kulmala et al., 2012).

$$203 J_{dp} = \frac{dN_{dp}}{dt} + CoagS_{dp} * N_{dp} + \frac{GR}{\Delta d_p} * N_{dp} \quad (\text{Eq. 1})$$

204 The first term dN_{dp}/dt is the change in concentration in the size bin, 5–9 nm. Ideally, this term, as well as the
205 concentration of particles within the size range, N_{dp} , in the following terms, are associated with the growth of
206 particles formed by atmospheric NPF past 5 nm; however, especially in traffic-related environments, they may also
207 have an unknown contribution by direct particle emissions to this respective size range (Okuljar et al., 2021;
208 Rönkkö et al., 2017). The second term $CoagS_{dp}$ is the coagulation sink, which describes the 5-9 nm particle losses
209 due to coagulation with larger particles calculated from the PNSD at each measurement site (Kulmala et al., 2012).
210 The third term describes the loss of particles due to their growth out of the size bin. Here, we calculated the growth
211 rates (GR) of 5–9 nm particles using the maximum concentration method (Kulmala et al., 2012) for days classified
212 as NPF event days as described by Dal Maso et al., (2005). The GR for non-event days was approximated using
213 the normalized PNSD from the sum of non-NPF events at each site. Such approximation is validated for several
214 locations as a ‘quiet NPF’ occurs with the similar GR as that on NPF event days (Kulmala et al., 2022a).

215 2.3.2 Extrapolation of particle formation rates

216 For Budapest and the Manacapuru (Amazonian basin), the particle formation rates were calculated from PNSD
217 measurements at 6 nm and 10 nm, respectively. Therefore, we obtained J_5 by extrapolating from J_6 and J_{10}
218 respectively. The J_5 extrapolation followed the analytical formula derived by Kerminen and Kulmala (2002). We
219 extrapolated J_5 from J_6 for Budapest. For Manacapuru, the extrapolations were done separately for J_{10} (wet season)
220 and J_{14} (dry season), due to the particle size limit of the measurement instrument.

221 2.3.3 Condensation and coagulation sink (CS and CoagS)

222 The CS and CoagS were calculated from the measured PNSD data for each site using the method proposed by
223 Kulmala et al., (2012). To ensure the comparability between all locations, both CS and CoagS were calculated
224 without the correction for hygroscopic growth. There are several ways to determine the hygroscopic growth factors
225 in CS and CoagS calculations. Laakso et al., (2004) developed parameterizations for Hyytiälä solely based on the
226 meteorological conditions and the aerosol composition in Hyytiälä, which results in the inapplicability of that
227 method to other sites. In the Supplementary of Baalbaki et al., (2021), Figure S4 shows the CS with hygroscopic
228 correction is about 1.1 – 1.3 times higher than dry CS, which would result in an overestimation on CS for the case
229 in Cyprus. Petters and Kreidenweis (2007) introduced the single hygroscopicity parameter κ (kappa), which can be
230 derived from Humidified Tandem Differential Mobility Analyzer (HTDMA) or cloud condensation nuclei counter
231 measurements or based on aerosol chemical composition obtained from instruments such as the Aerosol Chemical
232 Speciation Monitor (ACSM) or Aerosol Mass Spectrometers (AMS). In other locations, since organics are typically
233 the dominant component of aerosol mass in continental areas or marine polluted areas (Chen et al., 2022) and are
234 less hygroscopic than inorganics, one can expect an underestimation of CS similar to the one reported in (Baalbaki
235 et al., 2021). As a result, we omitted the hygroscopic growth impact for the chosen measurement sites to harmonize
236 the data composition and the later model analysis.

237 2.3.4 Datasets

238 The parameterizations were developed using the combined dataset from all six measurement sites in hourly time
239 resolution. Data points were selected considering detection limit of the instruments and therefore, the filters were
240 set to be $J_5 > 1 \times 10^{-5} \text{ cm}^{-3} \text{ s}^{-1}$, H_2SO_4 concentration $> 5 \times 10^3 \text{ cm}^{-3}$, $\text{RH} \in [0, 100] \%$ and $\text{CS} > 1 \times 10^{-5} \text{ s}^{-1}$. The complete
241 dataset was afterwards randomly resampled into a training set (75% from the complete dataset) and a testing set
242 (25% the rest of the complete dataset) for parameterization. In model testing, we included two additional inputs
243 from H_2SO_4 concentration proxies developed by Dada et al., (2020) from Hyytiälä and Beijing. The detailed number
244 of data points per site are shown in Table 1. The data distribution and comparison of each input variable are
245 displayed in Figure S2, where the overall variations of the input variables across the six sites are distinct in their
246 range and intensity, which pronounces the inclusivity of model training for a wider application in global
247 environments.

248

249 3 Parameterization of J_5

250 3.1 Derivation of parameterization models

251 We derived the parametrized J_5 based on the input variables (H_2SO_4 , RH, CS), which were chosen based on field
252 observations that highlighted their roles in the particle formation mechanism across various environments (Baalbaki
253 et al., 2021; Dada et al., 2020; Kerminen et al., 2018; Myers et al., 2022; Salma et al., 2016, 2021; Yan et al., 2021).
254 It has been discovered that NPF events occur favorably under lower RH, for example in boreal forests (Dada et al.,
255 2018; Yao et al., 2018), Mediterranean regions (Debevec et al., 2018), from CLOUD chamber experiment
256 (Duplissy et al., 2016) and model studies (Hamed et al., 2011). RH was shown to be seasonally related to cloudiness
257 and global radiation, so that a decreasing global radiation can lead to an increased RH and cloudiness within the
258 troposphere (Ruosteenoja and Räisänen, 2013). To reduce the model complexity, we opted to use RH as an indirect
259 indicator of global radiation. A lower CS facilitates the occurrence of NPF events even in contrasting environments
260 with distinct types of condensable vapor. For example, CS is a measure of a sink for anthropogenic vapors in a
261 megacity (Wang et al., 2011) and for biogenic vapors in a clean boreal forest (Dada et al., 2017; Tuovinen et al.,
262 2020), as well as a sink for growing sub-5 nm clusters and particles (Kulmala et al., 2017). When combined with
263 H_2SO_4 as an input variable, the evidently important sink effect of a pre-existing particle population on the ambient
264 H_2SO_4 concentration is implicitly transferred from CS to H_2SO_4 in our parameterization. Indirectly, CS may also
265 be associated, either causally or not, with 1) emissions or sinks of vapors other than H_2SO_4 participation in NPF or
266 particle growth, and 2) primary particle emissions from traffic, which would influence particle formation rates
267 estimated from observations using eq. 1. Furthermore, since we omit the influence of hygroscopic growth of
268 particles on CS, a fraction of real sink effect of CS is implicitly transformed to the variable RH in our
269 parameterization.

270 We tested with T as an input variable during model derivation and training. However, the modelled results did not
271 show improvement compared to the current parameterization, suggesting that T provided redundant information
272 for describing particle formation in the context of our model's global application.

273 Other than sulfuric acid, highly oxygenated organic molecules (HOMs) and ammonia (NH_3) have been discovered
274 to play a significant role in particle formation process (Bianchi et al., 2019; Lehtipalo et al., 2018). The possible
275 cluster types may include $\text{H}_2\text{SO}_4\text{-NH}_3\text{-H}_2\text{O}$ (Yu et al., 2018) and HNO_3 -related clusters such as $\text{HNO}_3\text{-H}_2\text{SO}_4\text{-NH}_3$
276 in the upper tropospheric particle nucleation (Wang et al., 2020, 2022, 2023). Yet, we are unable to include HOM
277 nor NH_3 concentrations owing to limited data availability from the chosen measurement sites. So far, long-term

measurements (> 1 year) of HOMs, matching the time range covered by other variables, are only available in Hyytiälä from a CI-API-ToF mass spectrometer. However, this is not the case at other sites, limiting our ability to have simultaneous HOMs data across all environments included in this study. Similarly, the NH₃ concentrations either did not cover the same time period as other variables or were unavailable for the other environments.

3.1.1 Different versions of the parameterization models

The derived model functional forms are as follows:

Model 1 (the baseline model, Eq. 2) presents the simplest particle formation mechanism based solely on the abundance of the precursor vapor H₂SO₄ concentrations in the atmosphere. The coefficient k_1 serves as a scaling coefficient that represents the activation rate of clusters in the presence of H₂SO₄ molecules during cluster formation (Kulmala et al., 2006; Paasonen et al., 2010).

$$J_5 = k_1 \times [\text{H}_2\text{SO}_4] \quad (\text{Eq. 2})$$

Model 2 (Eq. 3) introduces RH in addition to model 1 to partially represent the effect of the changing meteorological conditions relating to the global radiation and ambient water vapor content on J_5 in general in different types of environments (Dada et al., 2017; Hamed et al., 2011; Li et al., 2019). The coefficient k_2 serves as a scaling coefficient and shown as the activation efficiency of the nucleated clusters.

$$J_5 = k_2 \times [\text{H}_2\text{SO}_4] \times \text{RH}^{k_{\text{RH}}} \quad (\text{Eq. 3})$$

Model 3 (Eq. 4) includes, in addition to model 2, the factor CS. As discussed above, in our parameterization CS is connected not only to the sink of newly formed particles prior to their growth past 5 nm, but possibly also to sinks or sources of vapors other than H₂SO₄ participating in particle formation and growth and, in polluted environments, to sub-10 nm particle emissions from traffic. The coefficient k_3 serves as a scaling coefficient for the activation and survival efficiency of the nucleated clusters.

$$J_5 = k_3 \times [\text{H}_2\text{SO}_4] \times \text{RH}^{k_{\text{RH}}} \times \text{CS}^{k_{\text{CS}}} \quad (\text{Eq. 4})$$

Model 4 (Eq. 5), additionally accounts for the formation of H₂SO₄ multimers in the gas phase prior to cluster formation as assumed by the kinetic theory (McMurry and Friedlander, 1979), the coefficient k_{SA} represents the number of H₂SO₄ molecules (2, 3, 4, etc...). Therefore, k_4 in this case is not the activation coefficient anymore but includes both the collision frequency and the probability of a stable particle formation after the collision (Sihto et al., 2006; Weber et al., 1996).

$$J_5 = k_4 \times [\text{H}_2\text{SO}_4]^{k_{\text{SA}}} \times \text{RH}^{k_{\text{RH}}} \times \text{CS}^{k_{\text{CS}}} \quad (\text{Eq. 5})$$

306 3.2 Model training results

307 To derive a parametrized J_5 based on precursor and other input variables from the training dataset, we used the
308 “*fmincon*” optimization algorithm in MATLAB to retrieve the values of each coefficient (k_1 - k_4 , k_{SA} , k_{RH} and k_{CS})
309 from the training dataset. The coefficients obtained for each of the models can be found in Table 2. The derived
310 models with the optimized coefficients were applied to the testing datasets and compared with the observed J_5 and
311 the parametrized J_5 . We evaluated the performance of each model based on the data distribution, the resulting
312 deviation from observation and its uncertainty. To maintain the global model’s simplicity, the parameterization
313 covered both daytime and night-time data for all sites in all models.

314 Figure S3 presents the measured to modelled J_5 from model 1-4 using training dataset from six measurement sites,
315 including the slopes and coefficient of determination (R^2). Overall, by comparing model 1 (Fig. S3a) and model 2
316 (Fig. S3b), we observed an improvement in the model performance with the inclusion of RH. The R^2 value
317 improved from 0.28 to 0.44, and the slope increased from 0.29 to 0.56. This observation confirmed the importance
318 of considering meteorological impact when parameterizing J_5 . By further including CS in model 3, the model
319 improved further (Fig. S3c), with the R^2 increasing from 0.44 to 0.49, and the slope from 0.56 to 0.62. To further
320 introduce the kinetic theory and the formation of H_2SO_4 dimers and other multimers, we added an exponent over
321 H_2SO_4 in model 4 (Fig. S3d). This addition showed a further improved correlation and slope between the measured
322 or modeled data for the training datasets ($R^2 = 0.57$, slope = 0.76). In subsequent testing, model 4 generally
323 outperformed the other models (see section 4, Fig. 2).

324 3.3 Model evaluations

325 3.3.1 MAE and RMSE

326 We computed the mean absolute errors (MAE), root mean square errors (RMSE) for each model using the testing
327 dataset to gain a better understanding of the models’ performance. The numerical values of MAE and RMSE are
328 given in Table S3.

329 The MAE calculation equation is as follows:

$$330 \quad MAE = \frac{1}{n} \sum_{i=1}^n |y_i - \hat{y}_i| \quad (Eq. 6)$$

331 where n is the number of data points (here it is the total number of data points from testing set, see Table 1), y_i is
 332 the observed value, and \hat{y}_i denotes the predicted value. MAE measures the accuracy of models' prediction power,
 333 by quantifying the average magnitude of errors between observed and predicted values (Chai and Draxler, 2014).
 334 A lower model error is manifested by a lower MAE value.
 335 The RMSE is calculated as the square root of the difference between the measured (y_i) and predicted (\hat{y}_i) J_5 values
 336 normalized by the number of data points.

$$RMSE = \sqrt{\frac{1}{n} \sum_{i=1}^n (y_i - \hat{y}_i)^2}$$

(Eq. 7)

338 RMSE also measures the average magnitude of errors of models. However unlike MAE, RMSE squares the errors
 339 giving greater weight to larger errors and penalizing them more heavily (Chai and Draxler, 2014). Therefore, RMSE
 340 values reveal whether the models' performances are highly influenced by large prediction errors. Similar to MAE,
 341 lower RMSE values indicate better model performance.

342 Figure S4 (upper panel) depicts a declining trend of the overall MAE from models 1 to 4 (Eqs. 2-5). For the
 343 environmental types investigated in this study, the MAE values of the four models from all sites are lower than 1,
 344 indicating that the mean differences on the magnitude for J_5 are minor when utilizing the parameter settings from
 345 our models. However, Budapest stands out due to the apparent higher MAE, potentially highlighting the distinct
 346 NPF mechanism in Budapest compared to the other sites as well as the seasonal limitations on its data (spring 2018
 347 only).

348 The RMSE values increased as more parameters were added into the model, peaking for model 3 (Fig. S4, lower
 349 panel), even though model 3 can predict J_5 for multiple types of environments on a satisfactory level. We can see
 350 that from model 1 to model 2, the inclusion of RH increased the model errors more compared to the addition of CS
 351 from model 2 to model 3. However, the RMSE values dropped significantly when H_2SO_4 was allowed to vary with
 352 an exponent k_{SA} in model 4 in the presence of both RH and CS.

353 Based on the results summarized above, models 3 and 4 (Eqs. 4 & 5) seem to be the most promising for global J_5
 354 prediction among all model types owing to their low MAE values. However, the lower RMSE for model 4 showed
 355 its outperformance to model 3.

356 3.3.2 Akaike Information Criterion

357 The Akaike Information Criterion (AIC) is a statistical measure that helps to evaluate the goodness-of-fit of a
358 statistical model. We use AIC as an evaluation tool because it can evaluate models with different number of
359 parameters and complexities, ensuring a balanced assessment. Eventually, it allows us to select the model with the
360 best balance between the model complexity and goodness-of-fit. The parameters used to calculate the AIC for each
361 site are shown in Tables S4-S6. A lower AIC score indicates a superior goodness-of-fit and a lower tendency for
362 model overfitting. The relative likelihood term (L , $L = e^{(AIC_{min}-AIC_i)/2}$), calculated from AIC scores, reflects the
363 likelihood that the i th model minimizes information loss as compared to the model with the lowest AIC. A relative
364 likelihood of 1 suggests that the model outstands other models in minimizing information loss. For boreal forest
365 environments (Table. S4), and urban environments (Table. S5), both models 1 and 4 minimized information loss
366 the most. For rural regions, model 4 (Eq. 5) performs the best (Table. S6). Compared to the baseline model (model
367 1, Eq. 2), we find that H_2SO_4 is a more powerful parameter than RH or CS in all environments. However, in
368 Manacapuru, including RH and CS shows clearly an improved predictive accuracy in model 4 (Eq. 5).

369 4 Results and discussion

370 4.1 Parameterization testing results

371 The scatterplots (Fig. 2) demonstrate the overall performance of the parameterizations from the 4 models (Eqs. 2-
372 5) using the testing dataset. The overall and site-specific Pearson's coefficients, slopes from robust linear fit
373 between the measured and modelled J_5 , as well as the number of data points from the testing dataset, can be found
374 in Table 3. Overall, r increased significantly for model 2 and 3 (Fig. 2b & 2c, $r = 0.69$, $r = 0.71$) compared to model
375 1 (Fig. 2a, $r = 0.55$) as we include relative humidity and condensation sink as model parameters. Model 4 provides
376 the best linear fit results, implying that the model can predict an overall reliable estimation on J_5 in all the
377 investigated environment types (Fig. 2d, $r = 0.78$). It is notable that with the combined data sets, the condensation
378 sink receives a positive exponent in models 3 and 4 ($k_{CS} = 0.56$ and 0.67 , respectively), likely due to its association
379 with concentrations of other condensable vapors than H_2SO_4 and traffic emissions.

380 4.1.1 Boreal forests: Hyytiälä and Värriö

381 Given the boreal forest background, Hyytiälä and Värriö exhibited comparable variations in the distribution of
382 modelled J_5 values from the four model types. As shown in Figure 3, model 3 ((a3), (b3), (c3)) and model 4 ((a4),
383 (b4), (c4)) illustrated a more centered data distribution between the modelled and measured J_5 , which demonstrates
384 a potential favoring of NPF under low RH conditions, likely associated with increased global radiation for the
385 boreal forest environment (Dada et al., 2018; Hamed et al., 2011) and lower sinks for vapors and growing sub-5
386 nm particles (see Section 3.1). Notice that the mean H_2SO_4 concentration in Värriö is about twice as high as that in
387 Hyytiälä, opposite to CS which is clearly lower in Värriö (Table S2). The low CS in Värriö compared with Hyytiälä
388 is primarily due to the lower emission rate of the regional precursor vapors (e.g. Tunved et al., 2006), leading also
389 to the lower observed NPF event frequencies (Kyrö et al., 2014; Neefjes et al., 2022). We must note that the
390 Hyytiälä data spanned three years, containing more data points for model training, whereas the Värriö data only
391 covered the period from April to August 2019, excluding the entire cold season when H_2SO_4 concentrations are
392 significantly lower than those during the warm season (Jokinen et al., 2022). As a result, our model 3 (Fig. 3(a3),
393 (b3), (c3)) and 4 (Fig. 3(a4), (b4), (c4)) can predict J_5 for boreal forest environment on a satisfactory level, including
394 the possibility to use the estimated H_2SO_4 concentration from proxies as input. Nevertheless, limitations regarding
395 precursor vapor production rate could potentially influence the prediction accuracy.

396 4.1.2 Urban-influenced: Beijing and Budapest

397 In anthropogenic emissions dominated region, such as Beijing, the measured and modelled J_5 are well aligned
398 around the 1:1 line using model 3 (Fig. 3(d3), (e3), (f3)), and model 4 (Fig. 3 (d4), (e4), (f4)). In Beijing, a polluted
399 megacity, the dominating precursor type has been found to be H_2SO_4 -amine clusters (Cai et al., 2021). As expected,
400 the testing result showed dramatic underestimations for Beijing using model 1 with only H_2SO_4 concentrations
401 considered (Fig. 3(d1)), whereas models 2 (Fig. 3(d2)) and 3 (Fig. 3(d3)) yielded clearly enhanced J_5 predictions,
402 with relatively minor differences between models 2 and 3. These features are consistent with the fact that in addition
403 to H_2SO_4 , also other vapors are import to NPF and sub-5 nm particle growth in Beijing, and demonstrate that RH
404 and CS in our parameterization together determine in a complicated way the sources and sinks of these vapors, the
405 survival probability of sub-5 nm particles, and the potential emissions of sub-10 nm primary particles from traffic.
406 This study did not include amine-related compounds in the formulas because the lack of measured NH_3 data makes
407 the parallel comparisons difficult among the chosen sites for model training.

For Budapest, a large European city, the underestimates in modelled J_5 are not as much improved as they were for Beijing when including RH or CS in the parameterization, which is indicative of distinct particle formation pathways between Beijing and Budapest, even though both sites represent urban background environments. On one hand, it is worth noting that including RH (model 2, Eq. 3) resulted in a decrease in the correlation coefficients between the measured and modelled J_5 in Budapest from 0.54 to 0.46 (Table 3). This suggests that the role of RH in the NPF process in Budapest is less significant than other chosen inputs, despite previous indications that high RH levels have a strong potential to suppress NPF during non-event days in Budapest (Salma et al., 2021), even though the RH values in Budapest were considerably higher than those in Beijing (Table S2). On the other hand, including CS (model 3, Eq. 4) in addition to RH (model 2, Eq. 3) leads to an increase in the correlation coefficients between the measured and modelled J_5 from 0.46 to 0.61 (Table 3). We used both NPF and non-NPF days during model training even though it was found that CS was 50% lower during non-NPF events in Budapest than the values during NPF events (Salma et al., 2016). As a result, it is difficult to determine if the model's performance gain was entirely brought on by the addition of CS. Otherwise, the results are all in line with the earlier indirect evidence that chemical species other than H_2SO_4 influence the particle growth and possibly NPF process in Budapest (Salma and Németh, 2019). If one considers additional vapors other than H_2SO_4 for Budapest alone for J parameterization, one could include oxidation products of VOCs originating from either urban vegetation emissions or traffic emissions. For example, isoprene oxidation products can be used to describe the inhibiting effect on NPF (Heinritzi et al., 2020; Kiendler-Scharr et al., 2009), while monoterpene oxidation products could enhance sub-3 nm particle growth (Kulmala et al., 2013).

Based on the testing results, model 3 is more likely to predict a more accurate J_5 for Beijing based on the highest AIC ratio (except for 1), while model 1 predicts better for Budapest. Notice the fact that J_5 showed distinct levels of measured J_5 dependence with RH and CS in Beijing and Budapest (J_5 and RH: Beijing: $r = -0.21$, Budapest: $r = -0.1$; J_5 and CS: Beijing: $r = -0.02$, Budapest: $r = 0.57$, Fig. S1).

4.1.3 Mediterranean rural site: Agia Marina, Cyprus

For Cyprus, it appears that meteorology and condensation sink terms have only minor effects on the formation of 5 nm particles in such rural environment under the influence of marine vapors when comparing the results from testing dataset across models (Fig. 3g). However, including RH improves slightly the correlation between the modelled and measured J_5 as seen in model 2 (r rises from 0.42 to 0.49, Table 3). The reduced values of r in model 3 (Eq. 4) indicate a somewhat reversed impact of CS on J_5 , which requires additional examination as J_5 and CS are

weakly correlated ($r = 0.03$, Fig. S1). The H_2SO_4 concentration showed a low contribution to J_5 with the exponent being less than 1 in model 4 (Table 3), which led to a more underestimated modelled J_5 comparing to model 1 (Fig. 3(g1), (g4)). This could be an indication that potentially other anthropogenic, biogenic or marine compounds are of greater contribution to the particle formation processes in Cyprus than H_2SO_4 (Debevec et al., 2018). Owing to the orographic conditions, the air mass types approaching to the Cyprus measurement site are mixed, including the ones from North Africa, Marine, Europe, and northwest/southwest Asia. This results in the Mediterranean atmosphere in Agia Marina containing various vapors that could influence NPF. The potential key contributors could include oxidation products of dimethyl sulfide (DMS) originating from ocean plankton emissions (Rosati et al., 2021), iodine oxidation products like HIO_3 (He et al., 2021), the stabilizing agent NH_3 (Jiang and Xia, 2017; Lan et al., 2021; Lehtipalo et al., 2018; Yu et al., 2018), and oxidation products of VOCs from the surrounding pines forests and oaks under favorable meteorological conditions (Debevec et al., 2018). We should note that the measurements in Cyprus covered only two weeks in springtime, which limited our quantitative observations in model training for other seasons compared to sites with long-term measurements. Based on the findings above, model 1 seems to be the most suitable functional form for the prediction of J_5 in Cyprus.

4.1.4 Amazonian basin: Manacapuru, Brazil

The measured and modelled values of J_5 from the Manacapuru site scatter around the 1:1 line in all the models (Fig. 3). Previous studies reported high RH levels year-round in the measurement site near Manacapuru (Myers et al., 2022; Zhao et al., 2022), which is expected to suppress NPF frequency and to lead to lower formation rates. We observed such suppression effect when taking RH into account as shown by the increased correlation coefficients from 0.004 to 0.19 (Table 3). Studies from Manacapuru suggested that the epoxide vapors could be a potential precursor vapor in particle formation because of anthropogenic influences (Paulot et al., 2009), while Xu et al., (2014) suggested the presence of epoxide vapors can enhance particle nucleation when RH levels increase. We did not observe apparent improved model performance in model 3 when CS is included, as r remained almost unchanged compared to model 2 (Table 3). One factor to consider is that we did not apply hygroscopic growth factor when calculating CS for Manacapuru to maintain the consistency of the training dataset. However, the impact of RH on CS, particularly on the actual particle surface area available for H_2SO_4 uptake, seems to be significant for high RH environments like Manacapuru (Myers et al., 2022). Another assumption could be that even with the high CS, it is still low enough to allow sufficient precursor vapors contributing to NPF processes.

These current findings provide evidence for H₂SO₄ being an effective enough precursor for the particle formation at 5 nm in the atmosphere of Manacapuru (model 1, Fig 3(h1)). However, the RH stabilization effect on H₂SO₄ is not exerted necessarily, as RH remains at high values at around 89 ±13 % despite whether it is measured during wet season or dry season (Myers et al., 2022). With these observations, model 1 with a focus on the H₂SO₄ concentrations manages to predict *J*₅ well for biogenic vapor dominated environment like Manacapuru.

5 Tracer model 5 simulation

We simulated the particle number size distribution (PNSD) in EC-Earth global chemical transport model TM5-MP (Tracer Model 5, Massively Parallel version, details in supplement) by applying it with our *J*₅ model 1 and 4. Together, we compared our simulation results with the acid-organic binary homogeneous nucleation model from Riccobono et al., (2014):

$$J_{\text{Riccobono}} = k_m \times [\text{H}_2\text{SO}_4]^p \times [\text{BioOxOrg}]^q, \quad (\text{Eq. 8})$$

where $k_m = 3.27 \times 10^{-21} \text{ cm}^6 \text{ s}^{-1}$, $p = 2$ and $q = 1$.

The details of the 14 tested measurement stations are shown in Table S7. Note that the data from these 14 stations are independent from any training or testing datasets used in the previous sections of this paper. Here, we essentially compared the simulated and measured PNSD in three particle modes (nucleation, Aitken, accumulation) from the entire year 2018 to assess the simulation accuracy among global environments.

Figure 4 shows the comparisons of PNSD between the on-site measurements and the TM5-MP simulations. For biogenic environments, simulations using model 4 shows the closest particle number size distribution to the measured ones particularly in Aitken mode particles, promoting the sulfuric acid-based nucleation mechanism involving the source-sink-meteorology even for environment dominated by biogenic vapors. For the Arctic region, model 4 simulated particle concentrations are overall overestimated, while model 1 simulation shows better alignment of particle number concentrations around the Aitken mode. This might indicate that the nucleation process has a lower dependence on the variations of meteorology than we expected. For coastal environments, even though Utö (Baltic Sea Island) and La Réunion (southern hemisphere island) are located at different hemispheres and also have different geographical settings, the nucleation mechanisms from models 1 and 4 both show similar predictions on particle concentrations across particle modes, with larger underestimation in the accumulation mode for model 1. This once again validates the source-sink-meteorology mechanism in model 4. By observing the ratio between the simulated and measured particle number concentrations, we can quickly see that the sulfuric acid-based particle formation mechanisms with (model 4) or without (model 1) meteorology inputs have successfully

495 narrowed the gap between the simulations and observations across all particle modes, with significant
496 improvements for the nucleation mode (Fig. 5). The “Total” contains the simulated/measured particle number
497 concentrations ratio from all particle modes, and it is obviously seen that applying model 4 improves the overall
498 global PNSD simulation compared with the sulfuric acid-organic vapor binary model from (Riccobono et al., 2014).
499 This observation shows that including the RH and CS is needed for better understanding of the global particle
500 number size distributions.

501 **6 Conclusion**

502 The particle formation rate is one of the key characteristics in new particle formation studies. By utilizing distinct
503 field measurement data, we can model the particle formation rate and estimate the overall atmospheric aerosol
504 budget over different environments. We parameterized J_5 in four functional forms using the combined datasets
505 from six environments, covering boreal forests (Hyytiälä, Värriö), urban sites (a megacity of Beijing and a large
506 European city of Budapest) and rural environment (Cyprus, Manacapuru). The particle formation schemes involve
507 the main precursor vapor H_2SO_4 , relative humidity (RH) and condensation sink (CS). Due to the small number of
508 parameters and the diversity of environments included to generate the schemes, the roles of RH and CS are not
509 only related to their potential direct impact on J_5 , but also to sources and sinks of vapors other than H_2SO_4
510 contributing to formation and growth of sub-5 nm particles and to potential emissions of sub-10 nm particles, e.g.,
511 from traffic. Overall, our models showed improved performances as RH and CS were taken into consideration. The
512 model evaluations may suggest that particle formation mechanism is more sensitive to certain factors in specific
513 environments. Sulfuric acid is an effective precursor vapor in NPF processes for most of the measurement sites we
514 selected for model training. Nevertheless, relying solely on H_2SO_4 generally resulted in a weaker model
515 performance for environments where the NPF schemes are dominated by biogenic emissions. This suggests that
516 for developing globally applicable particle formation rate models, more precursor vapor types need to be included
517 alongside H_2SO_4 .

518 The purpose of the paper is twofold: first, to address the lack of knowledge regarding global particle formation
519 rates for particles at 5 nm and larger, and second, to provide a globally applicable semi-empirical parameterization
520 for the sulfuric acid-based neutral particle formation. The simplicity of the parameterization is demonstrated by
521 three factors. First, NPF is a widespread occurrence in various types of environments, where the characteristics of
522 particle formation share common mechanisms involving major precursor types and environmental factors. Second,
523 the main input H_2SO_4 concentrations data can be obtained from field measurements or proxies, from which the

524 contribution of H_2SO_4 to NPF can be directly compared among global sites. Third, we skip the microphysics
525 complexity of sub-5 nm particles, where the physical and chemical properties differ significantly from those that
526 are above 5 nm when discussing particle formation and growth.

527 The limited data availability from certain sites (less than 1 year), such as Budapest, Cyprus and Manacapuru, should
528 be noted when applying our models. Conclusions drawn from these sites can be more confidently applied to the
529 specific seasons covered in the model training, such as springs being more representable for Budapest and Cyprus,
530 and summer to early autumn for Manacapuru.

531 Overall, our parameterization findings show that our models including H_2SO_4 concentration, RH and CS can predict
532 J_5 on a satisfactory level for various environment types at once. Among the tested models, models 3 and 4 (Eqs. 4
533 and 5) can be utilized for predicting J_5 in a global scale if (1) the H_2SO_4 concentrations are known whether through
534 field measurement or proxies, (2) the meteorology parameter RH is monitored continuously, and (3) the particle
535 number size distributions are sufficient and assessed to yield CS. Some caution should be maintained when utilizing
536 these models for environments with very low RH and/or high CS, especially if the high CS is related to primary
537 particle emissions, as the associations between these model parameters and J_5 are complicated and multifaceted.
538 While the parameterizations presented in this study offer an improvement over previous approaches, further
539 development is needed to incorporate vapors important for NPF, such as iodine oxoacids, particularly in marine
540 environments.

541 *Author contributions.* Measurements: NS, RB, CY, LQ, TJ, IS, MV, TW. Data Analysis: XL, LD, MZ, NS, RB,
542 CY, LQ, IS, PZ. Results interpretation: XL, LD, PP, TN. Discussions: all co-authors. Writing: XL, LD, PP, V-MK,
543 TN. Comments and revisions: all co-authors.

544 *Data availability.* The datasets used in this study are now available on Zenodo:
545 <https://zenodo.org/records/15295592>. The data for the 14 global measurement sites are from EBAS database
546 (<https://ebas-data.nilu.no/>, last access 13.12.2024).

547 *Conflict of interests.* At least one of the (co-)authors is a member of the editorial board of Aerosol Research.

548 *Code availability.* The MATLAB code used for the parameterization training in this paper is available on Zenodo:
549 <https://zenodo.org/records/15295592>.

550

551 *Acknowledgements.* This work was supported by the European Research Council H2020 projects GASPARCON
 552 (Grant No. 714621), FORCeS (Grant No. 821205), and EMME-CARE (Grant No. 856612), by the Cyprus
 553 Government, by the Hungarian Research Development and Innovation Office (contract: Advanced 150835), by the
 554 Research Council of Finland with grant numbers 355330 and 360114, and by ACCC Flagship funded by the
 555 Research Council of Finland grant number 337549. L.D. received funding from the Swiss National Science
 556 Foundation (Ambizione grant number 216181). We are grateful to all the people who have contributed to the
 557 ambient measurements at measurement stations. The Finnish and Cypriot stations are part of the European research
 558 infrastructure ACTRIS. We acknowledge ACTRIS CiGas – Centre for Reactive Trace Gases In Situ Measurements
 559 and CAIS-ECAC – Centre for Aerosol In Situ Measurements for providing operational support to the aerosol and
 560 reactive trace gas instruments at the stations. We also thank Dr. James N. Smith for providing the GoAmazon2014/5
 561 data for Manacapuru.

562

563 **References**

- 564 Aalto, P., Hämeri, K., Becker, E., Weber, R., Salm, J., Mäkelä, J. M., Hoell, C., O’dowd, C. D., Hansson, H.-C., Väkevä, M.,
 565 Koponen, I. K., Buzorius, G., and Kulmala, M.: Physical characterization of aerosol particles during nucleation events, *Tellus*
 566 *B Chem. Phys. Meteorol.*, 53, 344–358, <https://doi.org/10.3402/tellusb.v53i4.17127>, 2001.
- 567 Baalbaki, R., Pikridas, M., Jokinen, T., Laurila, T., Dada, L., Bezantakos, S., Ahonen, L., Neitola, K., Maisser, A.,
 568 Bimenyimana, E., Christodoulou, A., Unga, F., Savvides, C., Lehtipalo, K., Kangasluoma, J., Biskos, G., Petäjä, T., Kerminen,
 569 V.-M., Sciare, J., and Kulmala, M.: Towards understanding the characteristics of new particle formation in the Eastern
 570 Mediterranean, *Atmospheric Chem. Phys.*, 21, 9223–9251, <https://doi.org/10.5194/acp-21-9223-2021>, 2021.
- 571 Bellouin, N., Quaas, J., Gryspeerdt, E., Kinne, S., Stier, P., Watson-Parris, D., Boucher, O., Carslaw, K. S., Christensen, M.,
 572 Daniau, A.-L., Dufresne, J.-L., Feingold, G., Fiedler, S., Forster, P., Gettelman, A., Haywood, J. M., Lohmann, U., Malavelle,
 573 F., Mauritsen, T., McCoy, D. T., Myhre, G., Mülmenstädt, J., Neubauer, D., Possner, A., Rugenstein, M., Sato, Y., Schulz,
 574 M., Schwartz, S. E., Sourdeval, O., Storelvmo, T., Toll, V., Winker, D., and Stevens, B.: Bounding Global Aerosol Radiative
 575 Forcing of Climate Change, *Rev. Geophys.*, 58, e2019RG000660, <https://doi.org/10.1029/2019RG000660>, 2020.
- 576 Bergman, T., Makkonen, R., Schrödner, R., Swietlicki, E., Phillips, V. T. J., Le Sager, P., and van Noije, T.: Description and
 577 evaluation of a secondary organic aerosol and new particle formation scheme within TM5-MP v1.2, *Geosci. Model Dev.*, 15,
 578 683–713, <https://doi.org/10.5194/gmd-15-683-2022>, 2022.
- 579 Bianchi, F., Kurtén, T., Riva, M., Mohr, C., Rissanen, M. P., Roldin, P., Berndt, T., Crounse, J. D., Wennberg, P. O., Mentel,
 580 T. F., Wildt, J., Junninen, H., Jokinen, T., Kulmala, M., Worsnop, D. R., Thornton, J. A., Donahue, N., Kjaergaard, H. G., and

581 Ehn, M.: Highly Oxygenated Organic Molecules (HOM) from Gas-Phase Autoxidation Involving Peroxy Radicals: A Key
582 Contributor to Atmospheric Aerosol, *Chem. Rev.*, 119, 3472–3509, <https://doi.org/10.1021/acs.chemrev.8b00395>, 2019.

583 Bousiotis, D., Pope, F. D., Beddows, D. C. S., Dall’Osto, M., Massling, A., Nøjgaard, J. K., Nordstrøm, C., Niemi, J. V.,
584 Portin, H., Petäjä, T., Perez, N., Alastuey, A., Querol, X., Kouvarakis, G., Mihalopoulos, N., Vratolis, S., Eleftheriadis, K.,
585 Wiedensohler, A., Weinhold, K., Merkel, M., Tuch, T., and Harrison, R. M.: A phenomenology of new particle formation
586 (NPF) at 13 European sites, *Atmospheric Chem. Phys.*, 21, 11905–11925, <https://doi.org/10.5194/acp-21-11905-2021>, 2021.

587 Brean, J., Beddows, D. C. S., Harrison, R. M., Song, C., Tunved, P., Ström, J., Krejci, R., Freud, E., Massling, A., Skov, H.,
588 Asmi, E., Lupi, A., and Dall’Osto, M.: Collective geographical ecoregions and precursor sources driving Arctic new particle
589 formation, *Atmospheric Chem. Phys.*, 23, 2183–2198, <https://doi.org/10.5194/acp-23-2183-2023>, 2023.

590 Cai, R., Yan, C., Yang, D., Yin, R., Lu, Y., Deng, C., Fu, Y., Ruan, J., Li, X., Kontkanen, J., Zhang, Q., Kangasluoma, J., Ma,
591 Y., Hao, J., Worsnop, D. R., Bianchi, F., Paasonen, P., Kerminen, V.-M., Liu, Y., Wang, L., Zheng, J., Kulmala, M., and Jiang,
592 J.: Sulfuric acid–amine nucleation in urban Beijing, *Atmospheric Chem. Phys.*, 21, 2457–2468, [https://doi.org/10.5194/acp-](https://doi.org/10.5194/acp-21-2457-2021)
593 21-2457-2021, 2021.

594 Cai, R., Deng, C., Stolzenburg, D., Li, C., Guo, J., Kerminen, V.-M., Jiang, J., Kulmala, M., and Kangasluoma, J.: Survival
595 probability of new atmospheric particles: closure between theory and measurements from 1.4 to 100 nm, *Atmospheric*
596 *Chem. Phys.*, 22, 14571–14587, <https://doi.org/10.5194/acp-22-14571-2022>, 2022.

597 Calvo, A. I., Alves, C., Castro, A., Pont, V., Vicente, A. M., and Fraile, R.: Research on aerosol sources and chemical
598 composition: Past, current and emerging issues, *Atmospheric Res.*, 120–121, 1–28,
599 <https://doi.org/10.1016/j.atmosres.2012.09.021>, 2013.

600 Chai, T. and Draxler, R. R.: Root mean square error (RMSE) or mean absolute error (MAE)? – Arguments against avoiding
601 RMSE in the literature, *Geosci. Model Dev.*, 7, 1247–1250, <https://doi.org/10.5194/gmd-7-1247-2014>, 2014.

602 Chang, L.-S., Schwartz, S. E., McGraw, R., and Lewis, E. R.: Sensitivity of aerosol properties to new particle formation
603 mechanism and to primary emissions in a continental-scale chemical transport model, *J. Geophys. Res. Atmospheres*, 114,
604 <https://doi.org/10.1029/2008JD011019>, 2009.

605 Chen, G., Canonaco, F., Tobler, A., Aas, W., Alastuey, A., Allan, J., Atabakhsh, S., Aurela, M., Baltensperger, U., Bougiatioti,
606 A., De Brito, J. F., Ceburnis, D., Chazeau, B., Chebaicheb, H., Daellenbach, K. R., Ehn, M., El Haddad, I., Eleftheriadis, K.,
607 Favez, O., Flentje, H., Font, A., Fossom, K., Freney, E., Gini, M., Green, D. C., Heikkinen, L., Herrmann, H., Kalogridis, A.-
608 C., Keernik, H., Lhotka, R., Lin, C., Lunder, C., Maasikmets, M., Manousakas, M. I., Marchand, N., Marin, C., Marmureanu,
609 L., Mihalopoulos, N., Močnik, G., Nęcki, J., O’Dowd, C., Ovadnevaite, J., Peter, T., Petit, J.-E., Pikridas, M., Matthew Platt,
610 S., Pokorná, P., Poulain, L., Priestman, M., Riffault, V., Rinaldi, M., Rózański, K., Schwarz, J., Sciare, J., Simon, L., Skiba,
611 A., Slowik, J. G., Sosedova, Y., Stavroulas, I., Styszko, K., Teinmaa, E., Timonen, H., Tremper, A., Vasilescu, J., Via, M.,
612 Vodička, P., Wiedensohler, A., Zografou, O., Cruz Minguillón, M., and Prévôt, A. S. H.: European aerosol phenomenology –
613 8: Harmonised source apportionment of organic aerosol using 22 Year-long ACSM/AMS datasets, *Environ. Int.*, 166, 107325,
614 <https://doi.org/10.1016/j.envint.2022.107325>, 2022.

615 Chu, B., Kerminen, V.-M., Bianchi, F., Yan, C., Petäjä, T., and Kulmala, M.: Atmospheric new particle formation in China,
616 *Atmospheric Chem. Phys.*, 19, 115–138, <https://doi.org/10.5194/acp-19-115-2019>, 2019.

617 Dada, L., Paasonen, P., Nieminen, T., Buenrostro Mazon, S., Kontkanen, J., Peräkylä, O., Lehtipalo, K., Hussein, T., Petäjä,
618 T., Kerminen, V.-M., Bäck, J., and Kulmala, M.: Long-term analysis of clear-sky new particle formation events and nonevents
619 in Hyytiälä, *Atmospheric Chem. Phys.*, 17, 6227–6241, <https://doi.org/10.5194/acp-17-6227-2017>, 2017.

620 Dada, L., Chellapermal, R., Buenrostro Mazon, S., Paasonen, P., Lampilahti, J., Manninen, H. E., Junninen, H., Petäjä, T.,
621 Kerminen, V.-M., and Kulmala, M.: Refined classification and characterization of atmospheric new-particle formation events
622 using air ions, *Atmospheric Chem. Phys.*, 18, 17883–17893, <https://doi.org/10.5194/acp-18-17883-2018>, 2018.

623 Dada, L., Ylivinkka, I., Baalbaki, R., Li, C., Guo, Y., Yan, C., Yao, L., Sarnela, N., Jokinen, T., Daellenbach, K. R., Yin, R.,
624 Deng, C., Chu, B., Nieminen, T., Wang, Y., Lin, Z., Thakur, R. C., Kontkanen, J., Stolzenburg, D., Sipilä, M., Hussein, T.,
625 Paasonen, P., Bianchi, F., Salma, I., Weidinger, T., Pikridas, M., Sciare, J., Jiang, J., Liu, Y., Petäjä, T., Kerminen, V.-M., and
626 Kulmala, M.: Sources and sinks driving sulfuric acid concentrations in contrasting environments: implications on proxy
627 calculations, *Atmospheric Chem. Phys.*, 20, 11747–11766, <https://doi.org/10.5194/acp-20-11747-2020>, 2020.

628 Dal Maso, M., Kulmala, M., Riipinen, I., and Wagner, R.: Formation and growth of fresh atmospheric aerosols: Eight years of
629 aerosol size distribution data from SMEAR II, Hyytiälä, Finland, *Boreal Environ. Res.*, 10, 323–336, 2005.

630 Debevec, C., Sauvage, S., Gros, V., Sellegri, K., Sciare, J., Pikridas, M., Stavroulas, I., Leonardis, T., Gaudion, V., Depelchin,
631 L., Fronval, I., Sarda-Esteve, R., Baisnée, D., Bonsang, B., Savvides, C., Vrekoussis, M., and Locoge, N.: Driving parameters
632 of biogenic volatile organic compounds and consequences on new particle formation observed at an eastern Mediterranean
633 background site, *Atmospheric Chem. Phys.*, 18, 14297–14325, <https://doi.org/10.5194/acp-18-14297-2018>, 2018.

634 Deng, C., Fu, Y., Dada, L., Yan, C., Cai, R., Yang, D., Zhou, Y., Yin, R., Lu, Y., Li, X., Qiao, X., Fan, X., Nie, W., Kontkanen,
635 J., Kangasluoma, J., Chu, B., Ding, A., Kerminen, V.-M., Paasonen, P., Worsnop, D. R., Bianchi, F., Liu, Y., Zheng, J., Wang,
636 L., Kulmala, M., and Jiang, J.: Seasonal Characteristics of New Particle Formation and Growth in Urban Beijing, *Environ.*
637 *Sci. Technol.*, 54, 8547–8557, <https://doi.org/10.1021/acs.est.0c00808>, 2020.

638 Deng, C., Cai, R., Yan, C., Zheng, J., and Jiang, J.: Formation and growth of sub-3 nm particles in megacities: impact of
639 background aerosols, *Faraday Discuss.*, 226, 348–363, <https://doi.org/10.1039/D0FD00083C>, 2021.

640 Ding, J., Dai, Q., Zhang, Y., Xu, J., Huangfu, Y., and Feng, Y.: Air humidity affects secondary aerosol formation in different
641 pathways, *Sci. Total Environ.*, 759, 143540, <https://doi.org/10.1016/j.scitotenv.2020.143540>, 2021.

642 Duplissy, J., Merikanto, J., Franchin, A., Tsagkogeorgas, G., Kangasluoma, J., Wimmer, D., Vuollekoski, H., Schobesberger,
643 S., Lehtipalo, K., Flagan, R. C., Brus, D., Donahue, N. M., Vehkamäki, H., Almeida, J., Amorim, A., Barmet, P., Bianchi, F.,
644 Breitenlechner, M., Dunne, E. M., Guida, R., Henschel, H., Junninen, H., Kirkby, J., Kürten, A., Kupc, A., Määttänen, A.,
645 Makhmutov, V., Mathot, S., Nieminen, T., Onnela, A., Praplan, A. P., Riccobono, F., Rondo, L., Steiner, G., Tome, A.,
646 Walther, H., Baltensperger, U., Carslaw, K. S., Dommen, J., Hansel, A., Petäjä, T., Sipilä, M., Stratmann, F., Vrtala, A.,
647 Wagner, P. E., Worsnop, D. R., Curtius, J., and Kulmala, M.: Effect of ions on sulfuric acid-water binary particle formation:

648 2. Experimental data and comparison with QC-normalized classical nucleation theory, *J. Geophys. Res. Atmospheres*, 121,
649 1752–1775, <https://doi.org/10.1002/2015JD023539>, 2016.

650 Eisele, F. L. and Tanner, D. J.: Measurement of the gas phase concentration of H₂SO₄ and methane sulfonic acid and estimates
651 of H₂SO₄ production and loss in the atmosphere, *J. Geophys. Res. Atmospheres*, 98, 9001–9010,
652 <https://doi.org/10.1029/93JD00031>, 1993.

653 Glasoe, W. A., Volz, K., Panta, B., Freshour, N., Bachman, R., Hanson, D. R., McMurry, P. H., and Jen, C.: Sulfuric acid
654 nucleation: An experimental study of the effect of seven bases, *J. Geophys. Res. Atmospheres*, 120, 1933–1950,
655 <https://doi.org/10.1002/2014JD022730>, 2015.

656 Gordon, H., Kirkby, J., Baltensperger, U., Bianchi, F., Breitenlechner, M., Curtius, J., Dias, A., Dommen, J., Donahue, N. M.,
657 Dunne, E. M., Duplissy, J., Ehrhart, S., Flagan, R. C., Frege, C., Fuchs, C., Hansel, A., Hoyle, C. R., Kulmala, M., Kürten, A.,
658 Lehtipalo, K., Makhmutov, V., Molteni, U., Rissanen, M. P., Stozhkov, Y., Tröstl, J., Tsagkogeorgas, G., Wagner, R.,
659 Williamson, C., Wimmer, D., Winkler, P. M., Yan, C., and Carslaw, K. S.: Causes and importance of new particle formation
660 in the present-day and preindustrial atmospheres, *J. Geophys. Res. Atmospheres*, 122, 8739–8760,
661 <https://doi.org/10.1002/2017JD026844>, 2017.

662 Hamed, A., Korhonen, H., Sihto, S.-L., Joutsensaari, J., Järvinen, H., Petäjä, T., Arnold, F., Nieminen, T., Kulmala, M., Smith,
663 J. N., Lehtinen, K. E. J., and Laaksonen, A.: The role of relative humidity in continental new particle formation, *J. Geophys.*
664 *Res. Atmospheres*, 116, <https://doi.org/10.1029/2010JD014186>, 2011.

665 Hari, P. and Kulmala, M.: Station for measuring Ecosystem-Atmosphere relations (SMEAR II), *Boreal Environ. Res.*, 10,
666 2005.

667 He, X.-C., Tham, Y. J., Dada, L., Wang, M., Finkenzeller, H., Stolzenburg, D., Iyer, S., Simon, M., Kürten, A., Shen, J., Rörup,
668 B., Rissanen, M., Schobesberger, S., Baalbaki, R., Wang, D. S., Koenig, T. K., Jokinen, T., Sarnela, N., Beck, L. J., Almeida,
669 J., Amanatidis, S., Amorim, A., Ataei, F., Baccarini, A., Bertozzi, B., Bianchi, F., Brilke, S., Caudillo, L., Chen, D., Chiu, R.,
670 Chu, B., Dias, A., Ding, A., Dommen, J., Duplissy, J., El Haddad, I., Gonzalez Carracedo, L., Granzin, M., Hansel, A.,
671 Heinritzi, M., Hofbauer, V., Junninen, H., Kangasluoma, J., Kemppainen, D., Kim, C., Kong, W., Krechmer, J. E., Kvashin,
672 A., Laitinen, T., Lamkaddam, H., Lee, C. P., Lehtipalo, K., Leiminger, M., Li, Z., Makhmutov, V., Manninen, H. E., Marie,
673 G., Marten, R., Mathot, S., Mauldin, R. L., Mentler, B., Möhler, O., Müller, T., Nie, W., Onnela, A., Petäjä, T., Pfeifer, J.,
674 Philippov, M., Ranjithkumar, A., Saiz-Lopez, A., Salma, I., Scholz, W., Schuchmann, S., Schulze, B., Steiner, G., Stozhkov,
675 Y., Tauber, C., Tomé, A., Thakur, R. C., Väisänen, O., Vazquez-Pufleau, M., Wagner, A. C., Wang, Y., Weber, S. K., Winkler,
676 P. M., Wu, Y., Xiao, M., Yan, C., Ye, Q., Ylisirniö, A., Zauner-Wieczorek, M., Zha, Q., Zhou, P., Flagan, R. C., Curtius, J.,
677 Baltensperger, U., Kulmala, M., Kerminen, V.-M., Kurtén, T., et al.: Role of iodine oxoacids in atmospheric aerosol nucleation,
678 *Science*, 371, 589–595, <https://doi.org/10.1126/science.abe0298>, 2021.

679 Heinritzi, M., Dada, L., Simon, M., Stolzenburg, D., Wagner, A. C., Fischer, L., Ahonen, L. R., Amanatidis, S., Baalbaki, R.,
680 Baccarini, A., Bauer, P. S., Baumgartner, B., Bianchi, F., Brilke, S., Chen, D., Chiu, R., Dias, A., Dommen, J., Duplissy, J.,
681 Finkenzeller, H., Frege, C., Fuchs, C., Garmash, O., Gordon, H., Granzin, M., El Haddad, I., He, X., Helm, J., Hofbauer, V.,

682 Hoyle, C. R., Kangasluoma, J., Keber, T., Kim, C., Kürten, A., Lamkaddam, H., Laurila, T. M., Lampilahti, J., Lee, C. P.,
 683 Lehtipalo, K., Leiminger, M., Mai, H., Makhmutov, V., Manninen, H. E., Marten, R., Mathot, S., Mauldin, R. L., Mentler, B.,
 684 Molteni, U., Müller, T., Nie, W., Nieminen, T., Onnela, A., Partoll, E., Passananti, M., Petäjä, T., Pfeifer, J., Pospisilova, V.,
 685 Quéléver, L. L. J., Rissanen, M. P., Rose, C., Schobesberger, S., Scholz, W., Scholze, K., Sipilä, M., Steiner, G., Stozhkov,
 686 Y., Tauber, C., Tham, Y. J., Vazquez-Pufleau, M., Virtanen, A., Vogel, A. L., Volkamer, R., Wagner, R., Wang, M., Weitz,
 687 L., Wimmer, D., Xiao, M., Yan, C., Ye, P., Zha, Q., Zhou, X., Amorim, A., Baltensperger, U., Hansel, A., Kulmala, M., Tomé,
 688 A., Winkler, P. M., Worsnop, D. R., Donahue, N. M., Kirkby, J., and Curtius, J.: Molecular understanding of the suppression
 689 of new-particle formation by isoprene, *Atmospheric Chem. Phys.*, 20, 11809–11821, [https://doi.org/10.5194/acp-20-11809-](https://doi.org/10.5194/acp-20-11809-2020)
 690 2020, 2020.

691 Hellmuth, O.: Columnar modelling of nucleation burst evolution in the convective boundary layer – first results from a
 692 feasibility study Part I: Modelling approach, *Atmospheric Chem. Phys.*, 6, 4175–4214, [https://doi.org/10.5194/acp-6-4175-](https://doi.org/10.5194/acp-6-4175-2006)
 693 2006, 2006.

694 Huijnen, V., Williams, J., van Weele, M., van Noije, T., Krol, M., Dentener, F., Segers, A., Houweling, S., Peters, W., de Laat,
 695 J., Boersma, F., Bergamaschi, P., van Velthoven, P., Le Sager, P., Eskes, H., Alkemade, F., Scheele, R., Nédélec, P., and Pätz,
 696 H.-W.: The global chemistry transport model TM5: description and evaluation of the tropospheric chemistry version 3.0,
 697 *Geosci. Model Dev.*, 3, 445–473, <https://doi.org/10.5194/gmd-3-445-2010>, 2010.

698 Jiang, B. and Xia, D.: Role identification of NH₃ in atmospheric secondary new particle formation in haze occurrence of
 699 China, *Atmos. Environ.*, 163, 107–117, <https://doi.org/10.1016/j.atmosenv.2017.05.035>, 2017.

700 Jokinen, T., Sipilä, M., Junninen, H., Ehn, M., Lönn, G., Hakala, J., Petäjä, T., Mauldin, R. L. I., Kulmala, M., and Worsnop,
 701 D. R.: Atmospheric sulphuric acid and neutral cluster measurements using CI-API-TOF, *Atmospheric Chem. Phys.*, 12, 4117–
 702 4125, <https://doi.org/10.5194/acp-12-4117-2012>, 2012.

703 Jokinen, T., Lehtipalo, K., Thakur, R. C., Ylivinkka, I., Neitola, K., Sarnela, N., Laitinen, T., Kulmala, M., Petäjä, T., and
 704 Sipilä, M.: Measurement report: Long-term measurements of aerosol precursor concentrations in the Finnish subarctic boreal
 705 forest, *Atmospheric Chem. Phys.*, 22, 2237–2254, <https://doi.org/10.5194/acp-22-2237-2022>, 2022.

706 Junninen, H., Ehn, M., Petäjä, T., Luosujärvi, L., Kotiaho, T., Kostianinen, R., Rohner, U., Gonin, M., Fuhrer, K., Kulmala, M.,
 707 and Worsnop, D. R.: A high-resolution mass spectrometer to measure atmospheric ion composition, *Atmospheric Meas. Tech.*,
 708 3, 1039–1053, <https://doi.org/10.5194/amt-3-1039-2010>, 2010.

709 Kerminen, V.-M. and Kulmala, M.: Analytical formulae connecting the “real” and the “apparent” nucleation rate and the nuclei
 710 number concentration for atmospheric nucleation events, *J. Aerosol Sci.*, 33, 609–622, [https://doi.org/10.1016/S0021-](https://doi.org/10.1016/S0021-8502(01)00194-X)
 711 8502(01)00194-X, 2002.

712 Kerminen, V.-M., Chen, X., Vakkari, V., Petäjä, T., Kulmala, M., and Bianchi, F.: Atmospheric new particle formation and
 713 growth: review of field observations, *Environ. Res. Lett.*, 13, 103003, <https://doi.org/10.1088/1748-9326/aadf3c>, 2018.

714 Kiendler-Scharr, A., Wildt, J., Maso, M. D., Hohaus, T., Kleist, E., Mentel, T. F., Tillmann, R., Uerlings, R., Schurr, U., and
 715 Wahner, A.: New particle formation in forests inhibited by isoprene emissions, *Nature*, 461, 381–384,
 716 <https://doi.org/10.1038/nature08292>, 2009.

717 Kirkby, J., Curtius, J., Almeida, J., Dunne, E., Duplissy, J., Ehrhart, S., Franchin, A., Gagné, S., Ickes, L., Kürten, A., Kupc,
 718 A., Metzger, A., Riccobono, F., Rondo, L., Schobesberger, S., Tsagkogeorgas, G., Wimmer, D., Amorim, A., Bianchi, F.,
 719 Breitenlechner, M., David, A., Dommen, J., Downard, A., Ehn, M., Flagan, R. C., Haider, S., Hansel, A., Hauser, D., Jud, W.,
 720 Junninen, H., Kreissl, F., Kvashin, A., Laaksonen, A., Lehtipalo, K., Lima, J., Lovejoy, E. R., Makhmutov, V., Mathot, S.,
 721 Mikkilä, J., Minginette, P., Mogo, S., Nieminen, T., Onnela, A., Pereira, P., Petäjä, T., Schnitzhofer, R., Seinfeld, J. H., Sipilä,
 722 M., Stozhkov, Y., Stratmann, F., Tomé, A., Vanhanen, J., Viisanen, Y., Vrtala, A., Wagner, P. E., Walther, H., Weingartner,
 723 E., Wex, H., Winkler, P. M., Carslaw, K. S., Worsnop, D. R., Baltensperger, U., and Kulmala, M.: Role of sulphuric acid,
 724 ammonia and galactic cosmic rays in atmospheric aerosol nucleation, *Nature*, 476, 429–433,
 725 <https://doi.org/10.1038/nature10343>, 2011.

726 Kleindienst, T. E.: Epoxying Isoprene Chemistry, *Science*, 325, 687–688, <https://doi.org/10.1126/science.1178324>, 2009.

727 Kulmala, M., Maso, M. D., Mäkelä, J. M., Pirjola, L., Väkevä, M., Aalto, P., Miikkulainen, P., Hämeri, K., and O’ Dowd, C.
 728 D.: On the formation, growth and composition of nucleation mode particles, *Tellus B*, 53, 479–490,
 729 <https://doi.org/10.1034/j.1600-0889.2001.530411.x>, 2001.

730 Kulmala, M., Vehkamäki, H., Petäjä, T., Dal Maso, M., Lauri, A., Kerminen, V.-M., Birmili, W., and McMurry, P. H.:
 731 Formation and growth rates of ultrafine atmospheric particles: a review of observations, *J. Aerosol Sci.*, 35, 143–176,
 732 <https://doi.org/10.1016/j.jaerosci.2003.10.003>, 2004.

733 Kulmala, M., Lehtinen, K. E. J., and Laaksonen, A.: Cluster activation theory as an explanation of the linear dependence
 734 between formation rate of 3nm particles and sulphuric acid concentration, *Atmospheric Chem. Phys.*, 6, 787–793,
 735 <https://doi.org/10.5194/acp-6-787-2006>, 2006.

736 Kulmala, M., Petäjä, T., Nieminen, T., Sipilä, M., Manninen, H. E., Lehtipalo, K., Dal Maso, M., Aalto, P. P., Junninen, H.,
 737 Paasonen, P., Riipinen, I., Lehtinen, K. E. J., Laaksonen, A., and Kerminen, V.-M.: Measurement of the nucleation of
 738 atmospheric aerosol particles, *Nat. Protoc.*, 7, 1651–1667, <https://doi.org/10.1038/nprot.2012.091>, 2012.

739 Kulmala, M., Kontkanen, J., Junninen, H., Lehtipalo, K., Manninen, H. E., Nieminen, T., Petäjä, T., Sipilä, M., Schobesberger,
 740 S., Rantala, P., Franchin, A., Jokinen, T., Järvinen, E., Äijälä, M., Kangasluoma, J., Hakala, J., Aalto, P. P., Paasonen, P.,
 741 Mikkilä, J., Vanhanen, J., Aalto, J., Hakola, H., Makkonen, U., Ruuskanen, T., Mauldin, R. L., Duplissy, J., Vehkamäki, H.,
 742 Bäck, J., Kortelainen, A., Riipinen, I., Kurtén, T., Johnston, M. V., Smith, J. N., Ehn, M., Mentel, T. F., Lehtinen, K. E. J.,
 743 Laaksonen, A., Kerminen, V.-M., and Worsnop, D. R.: Direct Observations of Atmospheric Aerosol Nucleation, *Science*, 339,
 744 943–946, <https://doi.org/10.1126/science.1227385>, 2013.

745 Kulmala, M., Kerminen, V.-M., Petäjä, T., J. Ding, A., and Wang, L.: Atmospheric gas-to-particle conversion: why NPF events
 746 are observed in megacities?, *Faraday Discuss.*, 200, 271–288, <https://doi.org/10.1039/C6FD00257A>, 2017.

747 Kulmala, M., Junninen, H., Dada, L., Salma, I., Weidinger, T., Thén, W., Vörösmarty, M., Komsaare, K., Stolzenburg, D.,
 748 Cai, R., Yan, C., Li, X., Deng, C., Jiang, J., Petäjä, T., Nieminen, T., and Kerminen, V.-M.: Quiet New Particle Formation in
 749 the Atmosphere, *Front. Environ. Sci.*, 10, 2022a.
 750 Kulmala, M., Cai, R., Stolzenburg, D., Zhou, Y., Dada, L., Guo, Y., Yan, C., Petäjä, T., Jiang, J., and Kerminen, V.-M.: The
 751 contribution of new particle formation and subsequent growth to haze formation, *Environ. Sci. Atmospheres*, 2, 352–361,
 752 <https://doi.org/10.1039/D1EA00096A>, 2022b.
 753 Kulmala, M., Cai, R., Ezhova, E., Deng, C., Stolzenburg, D., Dada, L., Guo, Y., Chao, Y., Peräkylä, O., Lintunen, A.,
 754 Nieminen, T., Kokkonen, T. V., Sarnela, N., and Kerminen, T. P. & V.-M.: Direct link between the characteristics of
 755 atmospheric new particle formation and Continental Biosphere-Atmosphere-Cloud-Climate (COBACC) feedback loop, *Boreal*
 756 *Environ. Res.*, 28, 1–13, 2023.
 757 Kürten, A., Rondo, L., Ehrhart, S., and Curtius, J.: Calibration of a Chemical Ionization Mass Spectrometer for the
 758 Measurement of Gaseous Sulfuric Acid, *J. Phys. Chem. A*, 116, 6375–6386, <https://doi.org/10.1021/jp212123n>, 2012.
 759 Kyrö, E.-M., Väänänen, R., Kerminen, V.-M., Virkkula, A., Petäjä, T., Asmi, A., Dal Maso, M., Nieminen, T., Juhola, S.,
 760 Shcherbinin, A., Riipinen, I., Lehtipalo, K., Keronen, P., Aalto, P. P., Hari, P., and Kulmala, M.: Trends in new particle
 761 formation in eastern Lapland, Finland: effect of decreasing sulfur emissions from Kola Peninsula, *Atmospheric Chem. Phys.*,
 762 14, 4383–4396, <https://doi.org/10.5194/acp-14-4383-2014>, 2014.
 763 Laakso, L., Petaja, T., Lehtinen, K. E. J., Kulmala, M., Paatero, J., Horrak, U., Tammet, H., and Joutsensaari, J.: Ion production
 764 rate in a boreal forest based on ion, particle and radiation measurements, *Atmos Chem Phys*, 11, 2004.
 765 Laarne, P., Amnell, E., Zaidan, M. A., Mikkonen, S., and Nieminen, T.: Exploring Non-Linear Dependencies in Atmospheric
 766 Data with Mutual Information, *Atmosphere*, 13, 1046, <https://doi.org/10.3390/atmos13071046>, 2022.
 767 Lan, Z., Lin, W., Pu, W., and Ma, Z.: Measurement report: Exploring NH₃ behavior in urban and
 768 suburban Beijing: comparison and implications, *Atmospheric Chem. Phys.*, 21, 4561–4573, [https://doi.org/10.5194/acp-21-](https://doi.org/10.5194/acp-21-4561-2021)
 769 4561-2021, 2021.
 770 Lee, S.-H., Gordon, H., Yu, H., Lehtipalo, K., Haley, R., Li, Y., and Zhang, R.: New Particle Formation in the Atmosphere:
 771 From Molecular Clusters to Global Climate, *J. Geophys. Res. Atmospheres*, 124, 7098–7146,
 772 <https://doi.org/10.1029/2018JD029356>, 2019.
 773 Lehtinen, K. E. J. and Kulmala, M.: A model for particle formation and growth in the atmosphere with molecular resolution
 774 in size, *Atmos Chem Phys*, 7, 2003.
 775 Lehtipalo, K., Yan, C., Dada, L., Bianchi, F., Xiao, M., Wagner, R., Stolzenburg, D., Ahonen, L. R., Amorim, A., Baccarini,
 776 A., Bauer, P. S., Baumgartner, B., Bergen, A., Bernhammer, A.-K., Breitenlechner, M., Brilke, S., Buchholz, A., Mazon, S.
 777 B., Chen, D., Chen, X., Dias, A., Dommen, J., Draper, D. C., Duplissy, J., Ehn, M., Finkenzeller, H., Fischer, L., Frege, C.,
 778 Fuchs, C., Garmash, O., Gordon, H., Hakala, J., He, X., Heikkinen, L., Heinritzi, M., Helm, J. C., Hofbauer, V., Hoyle, C. R.,
 779 Jokinen, T., Kangasluoma, J., Kerminen, V.-M., Kim, C., Kirkby, J., Kontkanen, J., Kürten, A., Lawler, M. J., Mai, H., Mathot,
 780 S., Mauldin, R. L., Molteni, U., Nichman, L., Nie, W., Nieminen, T., Ojdanic, A., Onnela, A., Passananti, M., Petäjä, T., Piel,

781 F., Pospisilova, V., Quéléver, L. L. J., Rissanen, M. P., Rose, C., Sarnela, N., Schallhart, S., Schuchmann, S., Sengupta, K.,
782 Simon, M., Sipilä, M., Tauber, C., Tomé, A., Tröstl, J., Väisänen, O., Vogel, A. L., Volkamer, R., Wagner, A. C., Wang, M.,
783 Weitz, L., Wimmer, D., Ye, P., Ylisirniö, A., Zha, Q., Carslaw, K. S., Curtius, J., Donahue, N. M., Flagan, R. C., Hansel, A.,
784 Riipinen, I., Virtanen, A., Winkler, P. M., Baltensperger, U., Kulmala, M., and Worsnop, D. R.: Multicomponent new particle
785 formation from sulfuric acid, ammonia, and biogenic vapors, *Sci. Adv.*, 4, eaau5363, <https://doi.org/10.1126/sciadv.aau5363>,
786 2018.

787 Li, X., Chee, S., Hao, J., Abbatt, J. P. D., Jiang, J., and Smith, J. N.: Relative humidity effect on the formation of highly
788 oxidized molecules and new particles during monoterpene oxidation, *Atmospheric Chem. Phys.*, 19, 1555–1570,
789 <https://doi.org/10.5194/acp-19-1555-2019>, 2019.

790 Liu, Q., Jia, X., Quan, J., Li, J., Li, X., Wu, Y., Chen, D., Wang, Z., and Liu, Y.: New positive feedback mechanism between
791 boundary layer meteorology and secondary aerosol formation during severe haze events, *Sci. Rep.*, 8, 6095,
792 <https://doi.org/10.1038/s41598-018-24366-3>, 2018.

793 Liu, Y., Yan, C., Feng, Z., Zheng, F., Fan, X., Zhang, Y., Li, C., Zhou, Y., Lin, Z., Guo, Y., Zhang, Y., Ma, L., Zhou, W., Liu,
794 Z., Dada, L., Dällenbach, K., Kontkanen, J., Cai, R., Chan, T., Chu, B., Du, W., Yao, L., Wang, Y., Cai, J., Kangasluoma, J.,
795 Kokkonen, T., Kujansuu, J., Rusanen, A., Deng, C., Fu, Y., Yin, R., Li, X., Lu, Y., Liu, Y., Lian, C., Yang, D., Wang, W., Ge,
796 M., Wang, Y., Worsnop, D. R., Junninen, H., He, H., Kerminen, V.-M., Zheng, J., Wang, L., Jiang, J., Petäjä, T., Bianchi, F.,
797 and Kulmala, M.: Continuous and comprehensive atmospheric observations in Beijing: a station to understand the complex
798 urban atmospheric environment, *Big Earth Data*, 4, 295–321, <https://doi.org/10.1080/20964471.2020.1798707>, 2020.

799 Määttänen, A., Merikanto, J., Henschel, H., Duplissy, J., Makkonen, R., Ortega, I. K., and Vehkamäki, H.: New
800 Parameterizations for Neutral and Ion-Induced Sulfuric Acid-Water Particle Formation in Nucleation and Kinetic Regimes, *J.*
801 *Geophys. Res. Atmospheres*, 123, 1269–1296, <https://doi.org/10.1002/2017JD027429>, 2018.

802 Marten, R., Xiao, M., Rörup, B., Wang, M., Kong, W., He, X.-C., Stolzenburg, D., Pfeifer, J., Marie, G., S. Wang, D., Scholz,
803 W., Baccarini, A., Ping Lee, C., Amorim, A., Baalbaki, R., M. Bell, D., Bertozzi, B., Caudillo, L., Chu, B., Dada, L., Duplissy,
804 J., Finkenzeller, H., Gonzalez Carracedo, L., Granzin, M., Hansel, A., Heinritzi, M., Hofbauer, V., Kempainen, D., Kürten,
805 A., Lampimäki, M., Lehtipalo, K., Makhmutov, V., E. Manninen, H., Mentler, B., Petäjä, T., Philippov, M., Shen, J., Simon,
806 M., Stozhkov, Y., Tomé, A., C. Wagner, A., Wang, Y., K. Weber, S., Wu, Y., Zauner-Wieczorek, M., Curtius, J., Kulmala,
807 M., Möhler, O., Volkamer, R., M. Winkler, P., R. Worsnop, D., Dommen, J., C. Flagan, R., Kirkby, J., M. Donahue, N.,
808 Lamkaddam, H., Baltensperger, U., and Haddad, I. E.: Survival of newly formed particles in haze conditions, *Environ. Sci.*
809 *Atmospheres*, 2, 491–499, <https://doi.org/10.1039/D2EA00007E>, 2022.

810 Martin, S. T., Artaxo, P., Machado, L. a. T., Manzi, A. O., Souza, R. a. F., Schumacher, C., Wang, J., Andreae, M. O., Barbosa,
811 H. M. J., Fan, J., Fisch, G., Goldstein, A. H., Guenther, A., Jimenez, J. L., Pöschl, U., Silva Dias, M. A., Smith, J. N., and
812 Wendisch, M.: Introduction: Observations and Modeling of the Green Ocean Amazon (GoAmazon2014/5), *Atmospheric*
813 *Chem. Phys.*, 16, 4785–4797, <https://doi.org/10.5194/acp-16-4785-2016>, 2016.

814 Mauldin III, R. L., Frost, G. J., Chen, G., Tanner, D. J., Prevot, A. S. H., Davis, D. D., and Eisele, F. L.: OH measurements
815 during the First Aerosol Characterization Experiment (ACE 1): Observations and model comparisons, *J. Geophys. Res.*
816 *Atmospheres*, 103, 16713–16729, <https://doi.org/10.1029/98JD00882>, 1998.

817 Mazon, S. B., Kontkanen, J., Manninen, H. E., Nieminen, T., Kerminen, V.-M., and Kulmala, M.: A long-term comparison of
818 nighttime cluster events and daytime ion formation in a boreal forest, 2016.

819 McMurry, P. H. and Friedlander, S. K.: New particle formation in the presence of an aerosol, *Atmospheric Environ.* 1967, 13,
820 1635–1651, [https://doi.org/10.1016/0004-6981\(79\)90322-6](https://doi.org/10.1016/0004-6981(79)90322-6), 1979.

821 Myers, D. C., Kim, S., Sjostedt, S., Guenther, A. B., Seco, R., Vega Bustillos, O., Tota, J., Souza, R. A. F., and Smith, J. N.:
822 Sulfuric acid in the Amazon basin: measurements and evaluation of existing sulfuric acid proxies, *Atmospheric Chem. Phys.*,
823 22, 10061–10076, <https://doi.org/10.5194/acp-22-10061-2022>, 2022.

824 Myllys, N., Kubečka, J., Besel, V., Alfaouri, D., Olenius, T., Smith, J. N., and Passananti, M.: Role of base strength, cluster
825 structure and charge in sulfuric-acid-driven particle formation, *Atmospheric Chem. Phys.*, 19, 9753–9768,
826 <https://doi.org/10.5194/acp-19-9753-2019>, 2019.

827 Neefjes, I., Laapas, M., Liu, Y., Medus, E., Miettunen, E., Ahonen, L., Quelever, L., Aalto, J., Bäck, J., Kerminen, V.-M.,
828 Lampilahti, J., Luoma, K., Mäki, M., Mammarella, I., Petäjä, T., Rätty, M., Sarnela, N., Ylivinkka, I., Hakala, S., Kulmala, M.,
829 Nieminen, T., and Lintunen, A.: 25 years of atmospheric and ecosystem measurements in a boreal forest - Seasonal variation
830 and responses to warm and dry years, *Boreal Environ. Res.*, 27, 1–31, 2022.

831 Nieminen, T., Paasonen, P., Manninen, H. E., Sellegri, K., Kerminen, V.-M., and Kulmala, M.: Parameterization of ion-
832 induced nucleation rates based on ambient observations, *Atmospheric Chem. Phys.*, 11, 3393–3402,
833 <https://doi.org/10.5194/acp-11-3393-2011>, 2011.

834 Nieminen, T., Yli-Juuti, T., Manninen, H. E., Petäjä, T., Kerminen, V.-M., and Kulmala, M.: Technical note: New particle
835 formation event forecasts during PEGASOS–Zeppelin Northern mission 2013 in Hyytiälä, Finland, *Atmospheric Chem. Phys.*,
836 15, 12385–12396, <https://doi.org/10.5194/acp-15-12385-2015>, 2015.

837 Nieminen, T., Kerminen, V.-M., Petäjä, T., Aalto, P. P., Arshinov, M., Asmi, E., Baltensperger, U., Beddows, D. C. S., Beukes,
838 J. P., Collins, D., Ding, A., Harrison, R. M., Henzing, B., Hooda, R., Hu, M., Hörrak, U., Kivekäs, N., Komsaare, K., Krejci,
839 R., Kristensson, A., Laakso, L., Laaksonen, A., Leaitch, W. R., Lihavainen, H., Mihalopoulos, N., Németh, Z., Nie, W.,
840 O’Dowd, C., Salma, I., Sellegri, K., Svenningsson, B., Swietlicki, E., Tunved, P., Ulevicius, V., Vakkari, V., Vana, M.,
841 Wiedensohler, A., Wu, Z., Virtanen, A., and Kulmala, M.: Global analysis of continental boundary layer new particle formation
842 based on long-term measurements, *Atmospheric Chem. Phys.*, 18, 14737–14756, <https://doi.org/10.5194/acp-18-14737-2018>,
843 2018.

844 Okuljar, M., Kuuluvainen, H., Kontkanen, J., Garmash, O., Olin, M., Niemi, J. V., Timonen, H., Kangasluoma, J., Tham, Y.
845 J., Baalbaki, R., Sipilä, M., Salo, L., Lintusaari, H., Portin, H., Teinilä, K., Aurela, M., Dal Maso, M., Rönkkö, T., Petäjä, T.,
846 and Paasonen, P.: Measurement report: The influence of traffic and new particle formation on the size distribution of 1–

800 nm particles in Helsinki – a street canyon and an urban background station comparison, *Atmospheric Chem. Phys.*, 21, 9931–9953, <https://doi.org/10.5194/acp-21-9931-2021>, 2021.

Paasonen, P., Nieminen, T., Asmi, E., Manninen, H. E., Petäjä, T., Plass-Dülmer, C., Flentje, H., Birmili, W., Wiedensohler, A., Hörrak, U., Metzger, A., Hamed, A., Laaksonen, A., Facchini, M. C., Kerminen, V.-M., and Kulmala, M.: On the roles of sulphuric acid and low-volatility organic vapours in the initial steps of atmospheric new particle formation, *Atmospheric Chem. Phys.*, 10, 11223–11242, <https://doi.org/10.5194/acp-10-11223-2010>, 2010.

Paulot, F., Crounse, J. D., Kjaergaard, H. G., Kürten, A., St. Clair, J. M., Seinfeld, J. H., and Wennberg, P. O.: Unexpected Epoxide Formation in the Gas-Phase Photooxidation of Isoprene, *Science*, 325, 730–733, <https://doi.org/10.1126/science.1172910>, 2009.

Petters, M. D. and Kreidenweis, S. M.: A single parameter representation of hygroscopic growth and cloud condensation nucleus activity, *Atmospheric Chem. Phys.*, 7, 1961–1971, <https://doi.org/10.5194/acp-7-1961-2007>, 2007.

Quéléver, L. L. J., Dada, L., Asmi, E., Lampilahti, J., Chan, T., Ferrara, J. E., Copes, G. E., Pérez-Fogwill, G., Barreira, L., Aurela, M., Worsnop, D. R., Jokinen, T., and Sipilä, M.: Investigation of new particle formation mechanisms and aerosol processes at Marambio Station, Antarctic Peninsula, *Atmospheric Chem. Phys.*, 22, 8417–8437, <https://doi.org/10.5194/acp-22-8417-2022>, 2022.

Riccobono, F., Schobesberger, S., Scott, C. E., Dommen, J., Ortega, I. K., Rondo, L., Almeida, J., Amorim, A., Bianchi, F., Breitenlechner, M., David, A., Downard, A., Dunne, E. M., Duplissy, J., Ehrhart, S., Flagan, R. C., Franchin, A., Hansel, A., Junninen, H., Kajos, M., Keskinen, H., Kupc, A., Kürten, A., Kvashin, A. N., Laaksonen, A., Lehtipalo, K., Makhmutov, V., Mathot, S., Nieminen, T., Onnela, A., Petäjä, T., Praplan, A. P., Santos, F. D., Schallhart, S., Seinfeld, J. H., Sipilä, M., Spracklen, D. V., Stozhkov, Y., Stratmann, F., Tomé, A., Tsagkogeorgas, G., Vaattovaara, P., Viisanen, Y., Vrtala, A., Wagner, P. E., Weingartner, E., Wex, H., Wimmer, D., Carslaw, K. S., Curtius, J., Donahue, N. M., Kirkby, J., Kulmala, M., Worsnop, D. R., and Baltensperger, U.: Oxidation Products of Biogenic Emissions Contribute to Nucleation of Atmospheric Particles, *Science*, 344, 717–721, <https://doi.org/10.1126/science.1243527>, 2014.

Roldin, P., Swietlicki, E., Massling, A., Kristensson, A., Löndahl, J., Eriksson, A., Pagels, J., and Gustafsson, S.: Aerosol ageing in an urban plume – implication for climate, *Atmospheric Chem. Phys.*, 11, 5897–5915, <https://doi.org/10.5194/acp-11-5897-2011>, 2011.

Rönkkö, T., Kuuluvainen, H., Karjalainen, P., Keskinen, J., Hillamo, R., Niemi, J. V., Pirjola, L., Timonen, H. J., Saarikoski, S., Saukko, E., Järvinen, A., Silvennoinen, H., Rostedt, A., Olin, M., Yli-Ojanperä, J., Nousiainen, P., Kousa, A., and Dal Maso, M.: Traffic is a major source of atmospheric nanocluster aerosol, *Proc. Natl. Acad. Sci.*, 114, 7549–7554, <https://doi.org/10.1073/pnas.1700830114>, 2017.

Rosati, B., Christiansen, S., Wollesen de Jonge, R., Roldin, P., Jensen, M. M., Wang, K., Moosakutty, S. P., Thomsen, D., Salomonsen, C., Hyttinen, N., Elm, J., Feilberg, A., Glasius, M., and Bilde, M.: New Particle Formation and Growth from Dimethyl Sulfide Oxidation by Hydroxyl Radicals, *ACS Earth Space Chem.*, 5, 801–811, <https://doi.org/10.1021/acsearthspacechem.0c00333>, 2021.

881 Ruosteenoja, K. and Räisänen, P.: Seasonal Changes in Solar Radiation and Relative Humidity in Europe in Response to
882 Global Warming, *J. Clim.*, 26, 2467–2481, <https://doi.org/10.1175/JCLI-D-12-00007.1>, 2013.

883 Salma, I. and Németh, Z.: Dynamic and timing properties of new aerosol particle formation and consecutive growth events,
884 *Atmospheric Chem. Phys.*, 19, 5835–5852, <https://doi.org/10.5194/acp-19-5835-2019>, 2019.

885 Salma, I., Borsós, T., Weidinger, T., Aalto, P., Hussein, T., Dal Maso, M., and Kulmala, M.: Production, growth and properties
886 of ultrafine atmospheric aerosol particles in an urban environment, *Atmospheric Chem. Phys.*, 11, 1339–1353,
887 <https://doi.org/10.5194/acp-11-1339-2011>, 2011.

888 Salma, I., Németh, Z., Kerminen, V.-M., Aalto, P., Nieminen, T., Weidinger, T., Molnár, Á., Imre, K., and Kulmala, M.:
889 Regional effect on urban atmospheric nucleation, *Atmospheric Chem. Phys.*, 16, 8715–8728, [https://doi.org/10.5194/acp-16-](https://doi.org/10.5194/acp-16-8715-2016)
890 8715-2016, 2016.

891 Salma, I., Thén, W., Aalto, P., Kerminen, V.-M., Kern, A., Barcza, Z., Petäjä, T., and Kulmala, M.: Influence of vegetation on
892 occurrence and time distributions of regional new aerosol particle formation and growth, *Atmospheric Chem. Phys.*, 21, 2861–
893 2880, <https://doi.org/10.5194/acp-21-2861-2021>, 2021.

894 Sanchez, K. J., Russell, L. M., Modini, R. L., Frossard, A. A., Ahlm, L., Corrigan, C. E., Roberts, G. C., Hawkins, L. N.,
895 Schroder, J. C., Bertram, A. K., Zhao, R., Lee, A. K. Y., Lin, J. J., Nenes, A., Wang, Z., Wonaschütz, A., Sorooshian, A.,
896 Noone, K. J., Jonsson, H., Toom, D., Macdonald, A. M., Leaitch, W. R., and Seinfeld, J. H.: Meteorological and aerosol effects
897 on marine cloud microphysical properties, *J. Geophys. Res. Atmospheres*, 121, 4142–4161,
898 <https://doi.org/10.1002/2015JD024595>, 2016.

899 Schiro, K. A., Ahmed, F., Giangrande, S. E., and Neelin, J. D.: GoAmazon2014/5 campaign points to deep-inflow approach
900 to deep convection across scales, *Proc. Natl. Acad. Sci.*, 115, 4577–4582, <https://doi.org/10.1073/pnas.1719842115>, 2018.

901 Sihto, S.-L., Kulmala, M., Kerminen, V.-M., Dal Maso, M., Petäjä, T., Riipinen, I., Korhonen, H., Arnold, F., Janson, R., Boy,
902 M., Laaksonen, A., and Lehtinen, K. E. J.: Atmospheric sulphuric acid and aerosol formation: implications from atmospheric
903 measurements for nucleation and early growth mechanisms, *Atmospheric Chem. Phys.*, 6, 4079–4091,
904 <https://doi.org/10.5194/acp-6-4079-2006>, 2006.

905 Spracklen, D. V., Bonn, B., and Carslaw, K. S.: Boreal forests, aerosols and the impacts on clouds and climate, *Philos. Trans.*
906 *R. Soc. Math. Phys. Eng. Sci.*, 366, 4613–4626, <https://doi.org/10.1098/rsta.2008.0201>, 2008.

907 Tunved, P., Hansson, H.-C., Kerminen, V.-M., Ström, J., Maso, M. D., Lihavainen, H., Viisanen, Y., Aalto, P. P., Komppula,
908 M., and Kulmala, M.: High Natural Aerosol Loading over Boreal Forests, *Science*, 312, 261–263,
909 <https://doi.org/10.1126/science.1123052>, 2006.

910 Tuovinen, S., Kontkanen, J., Jiang, J., and Kulmala, M.: Investigating the effectiveness of condensation sink based on
911 heterogeneous nucleation theory, *J. Aerosol Sci.*, 149, 105613, <https://doi.org/10.1016/j.jaerosci.2020.105613>, 2020.

912 Tuovinen, S., Cai, R., Kerminen, V.-M., Jiang, J., Yan, C., Kulmala, M., and Kontkanen, J.: Survival probabilities of
913 atmospheric particles: comparison based on theory, cluster population simulations, and observations in Beijing, *Atmospheric*
914 *Chem. Phys.*, 22, 15071–15091, <https://doi.org/10.5194/acp-22-15071-2022>, 2022.

915 Uno, I., Wang, Z., Itahashi, S., Yumimoto, K., Yamamura, Y., Yoshino, A., Takami, A., Hayasaki, M., and Kim, B.-G.:
 916 Paradigm shift in aerosol chemical composition over regions downwind of China, *Sci. Rep.*, 10, 6450,
 917 <https://doi.org/10.1038/s41598-020-63592-6>, 2020.

918 Wang, M., Kong, W., Marten, R., He, X.-C., Chen, D., Pfeifer, J., Heitto, A., Kontkanen, J., Dada, L., Kürten, A., Yli-Juuti,
 919 T., Manninen, H. E., Amanatidis, S., Amorim, A., Baalbaki, R., Baccarini, A., Bell, D. M., Bertozzi, B., Bräkling, S., Brilke,
 920 S., Murillo, L. C., Chiu, R., Chu, B., De Menezes, L.-P., Duplissy, J., Finkenzeller, H., Carracedo, L. G., Granzin, M., Guida,
 921 R., Hansel, A., Hofbauer, V., Krechmer, J., Lehtipalo, K., Lamkaddam, H., Lampimäki, M., Lee, C. P., Makhmutov, V., Marie,
 922 G., Mathot, S., Mauldin, R. L., Mentler, B., Müller, T., Onnela, A., Partoll, E., Petäjä, T., Philippov, M., Pospisilova, V.,
 923 Ranjithkumar, A., Rissanen, M., Rörup, B., Scholz, W., Shen, J., Simon, M., Sipilä, M., Steiner, G., Stolzenburg, D., Tham,
 924 Y. J., Tomé, A., Wagner, A. C., Wang, D. S., Wang, Y., Weber, S. K., Winkler, P. M., Wlasits, P. J., Wu, Y., Xiao, M., Ye,
 925 Q., Zauner-Wieczorek, M., Zhou, X., Volkamer, R., Riipinen, I., Dommen, J., Curtius, J., Baltensperger, U., Kulmala, M.,
 926 Worsnop, D. R., Kirkby, J., Seinfeld, J. H., El-Haddad, I., Flagan, R. C., and Donahue, N. M.: Rapid growth of new
 927 atmospheric particles by nitric acid and ammonia condensation, *Nature*, 581, 184–189, [https://doi.org/10.1038/s41586-020-](https://doi.org/10.1038/s41586-020-2270-4)
 928 [2270-4](https://doi.org/10.1038/s41586-020-2270-4), 2020.

929 Wang, M., Xiao, M., Bertozzi, B., Marie, G., Rörup, B., Schulze, B., Bardakov, R., He, X.-C., Shen, J., Scholz, W., Marten,
 930 R., Dada, L., Baalbaki, R., Lopez, B., Lamkaddam, H., Manninen, H. E., Amorim, A., Ataei, F., Bogert, P., Brasseur, Z.,
 931 Caudillo, L., De Menezes, L.-P., Duplissy, J., Ekman, A. M. L., Finkenzeller, H., Carracedo, L. G., Granzin, M., Guida, R.,
 932 Heinritzi, M., Hofbauer, V., Höhler, K., Korhonen, K., Krechmer, J. E., Kürten, A., Lehtipalo, K., Mahfouz, N. G. A.,
 933 Makhmutov, V., Massabò, D., Mathot, S., Mauldin, R. L., Mentler, B., Müller, T., Onnela, A., Petäjä, T., Philippov, M.,
 934 Piedehierro, A. A., Pozzer, A., Ranjithkumar, A., Schervish, M., Schobesberger, S., Simon, M., Stozhkov, Y., Tomé, A., Umo,
 935 N. S., Vogel, F., Wagner, R., Wang, D. S., Weber, S. K., Welti, A., Wu, Y., Zauner-Wieczorek, M., Sipilä, M., Winkler, P.
 936 M., Hansel, A., Baltensperger, U., Kulmala, M., Flagan, R. C., Curtius, J., Riipinen, I., Gordon, H., Lelieveld, J., El-Haddad,
 937 I., Volkamer, R., Worsnop, D. R., Christoudias, T., Kirkby, J., Möhler, O., and Donahue, N. M.: Synergistic HNO₃–H₂SO₄–
 938 NH₃ upper tropospheric particle formation, *Nature*, 605, 483–489, <https://doi.org/10.1038/s41586-022-04605-4>, 2022.

939 Wang, S., Peng, Y., Zhang, Q., Wang, W., and Wang, Q.: Mechanistic understanding of rapid H₂SO₄-HNO₃-NH₃ nucleation
 940 in the upper troposphere, *Sci. Total Environ.*, 883, 163477, <https://doi.org/10.1016/j.scitotenv.2023.163477>, 2023.

941 Wang, Z. B., Hu, M., Yue, D. L., Zheng, J., Zhang, R. Y., Wiedensohler, A., Wu, Z. J., Nieminen, T., and Boy, M.: Evaluation
 942 on the role of sulfuric acid in the mechanisms of new particle formation for Beijing case, *Atmospheric Chem. Phys.*, 11, 12663–
 943 12671, <https://doi.org/10.5194/acp-11-12663-2011>, 2011.

944 Weber, R., Marti, J., McMurry, P., Eisele, F., Tanner, D., and Jefferson, A.: Measured atmospheric new particle formation
 945 rates: Implications for nucleation mechanisms, *Chem. Eng. Commun.*, 151, 53–64,
 946 <https://doi.org/10.1080/00986449608936541>, 1996.

947 Xu, W., Gomez-Hernandez, M., Guo, S., Secretst, J., Marrero-Ortiz, W., Zhang, A. L., and Zhang, R.: Acid-Catalyzed
 948 Reactions of Epoxides for Atmospheric Nanoparticle Growth, *J. Am. Chem. Soc.*, 136, 15477–15480,
 949 <https://doi.org/10.1021/ja508989a>, 2014.

950 Yan, C., Yin, R., Lu, Y., Dada, L., Yang, D., Fu, Y., Kontkanen, J., Deng, C., Garmash, O., Ruan, J., Baalbaki, R., Schervish,
 951 M., Cai, R., Bloss, M., Chan, T., Chen, T., Chen, Q., Chen, X., Chen, Y., Chu, B., Dällenbach, K., Foreback, B., He, X.,
 952 Heikkinen, L., Jokinen, T., Junninen, H., Kangasluoma, J., Kokkonen, T., Kurppa, M., Lehtipalo, K., Li, H., Li, H., Li, X.,
 953 Liu, Y., Ma, Q., Paasonen, P., Rantala, P., Pileci, R. E., Rusanen, A., Sarnela, N., Simonen, P., Wang, S., Wang, W., Wang,
 954 Y., Xue, M., Yang, G., Yao, L., Zhou, Y., Kujansuu, J., Petäjä, T., Nie, W., Ma, Y., Ge, M., He, H., Donahue, N. M., Worsnop,
 955 D. R., Kerminen, V.-M., Wang, L., Liu, Y., Zheng, J., Kulmala, M., Jiang, J., and Bianchi, F.: The Synergistic Role of Sulfuric
 956 Acid, Bases, and Oxidized Organics Governing New-Particle Formation in Beijing, *Geophys. Res. Lett.*, 48, e2020GL091944,
 957 <https://doi.org/10.1029/2020GL091944>, 2021.

958 Yao, L., Garmash, O., Bianchi, F., Zheng, J., Yan, C., Kontkanen, J., Junninen, H., Mazon, S. B., Ehn, M., Paasonen, P., Sipilä,
 959 M., Wang, M., Wang, X., Xiao, S., Chen, H., Lu, Y., Zhang, B., Wang, D., Fu, Q., Geng, F., Li, L., Wang, H., Qiao, L., Yang,
 960 X., Chen, J., Kerminen, V.-M., Petäjä, T., Worsnop, D. R., Kulmala, M., and Wang, L.: Atmospheric new particle formation
 961 from sulfuric acid and amines in a Chinese megacity, *Science*, 361, 278–281, <https://doi.org/10.1126/science.aao4839>, 2018.

962 Yli-Juuti, T., Riipinen, I., Aalto, P. P., Nieminen, T., Maenhaut, W., Janssens, I. A., Claeys, M., Salma, I., Ocskay, R., Hoffer,
 963 A., Imre, K., and Kulmala, M.: Characteristics of new particle formation events and cluster ions at K-puszt, Hungary, 2009.

964 Yu, F., Nadykto, A. B., Herb, J., Luo, G., Nazarenko, K. M., and Uvarova, L. A.: $\text{H}_2\text{SO}_4\text{--H}_2\text{O--NH}_3$ ternary ion-mediated
 965 nucleation (TIMN): kinetic-based model and comparison with CLOUD measurements, *Atmospheric Chem. Phys.*, 18, 17451–
 966 17474, <https://doi.org/10.5194/acp-18-17451-2018>, 2018.

967 Zaidan, M. A., Haapasilta, V., Relan, R., Paasonen, P., Kerminen, V.-M., Junninen, H., Kulmala, M., and Foster, A. S.:
 968 Exploring non-linear associations between atmospheric new-particle formation and ambient variables: a mutual information
 969 approach, *Atmospheric Chem. Phys.*, 18, 12699–12714, <https://doi.org/10.5194/acp-18-12699-2018>, 2018.

970 Zhang, Y., McMurry, P. H., Yu, F., and Jacobson, M. Z.: A comparative study of nucleation parameterizations: 1. Examination
 971 and evaluation of the formulations, *J. Geophys. Res. Atmospheres*, 115, <https://doi.org/10.1029/2010JD014150>, 2010.

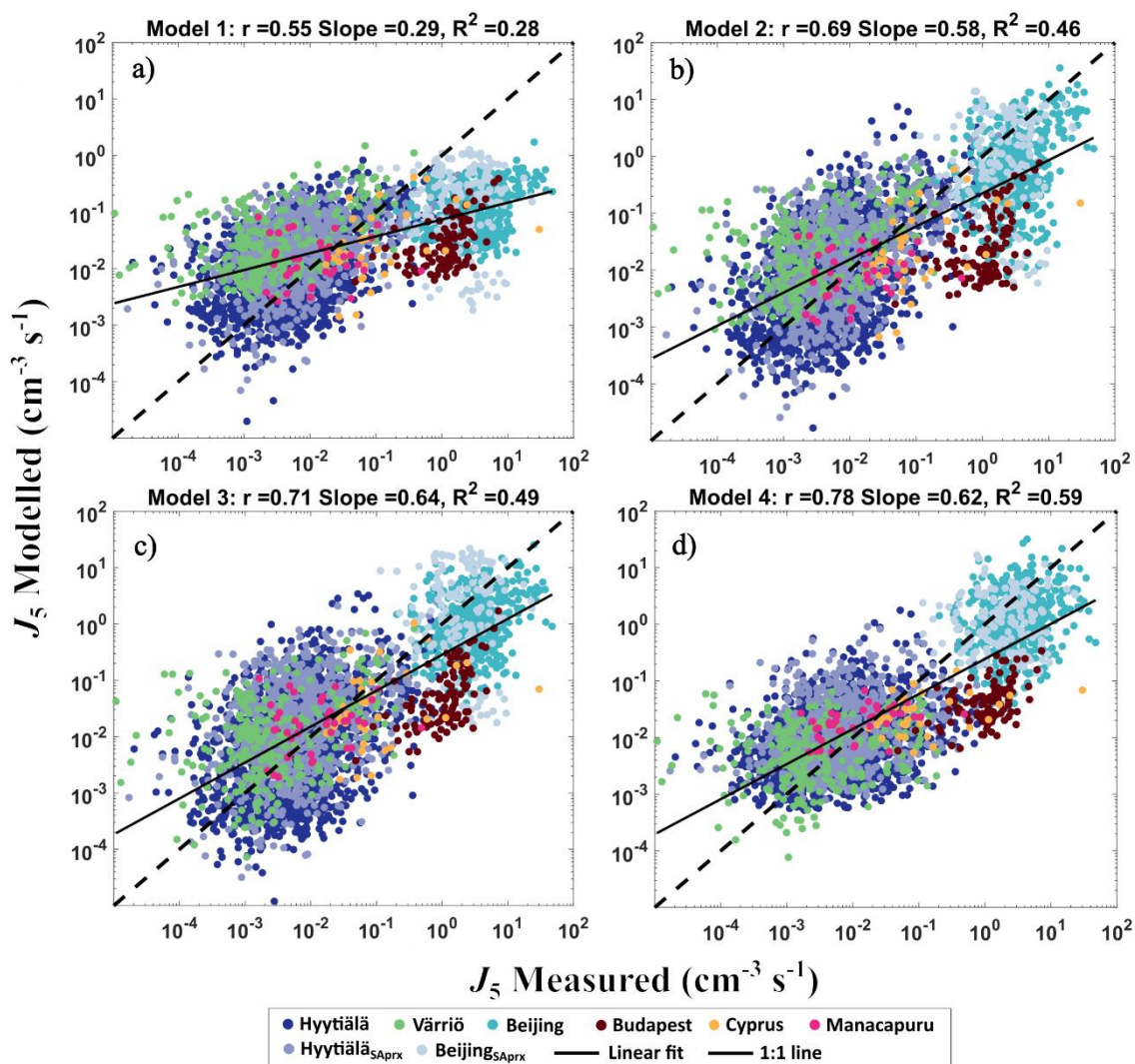
972 Zhao, B., Fast, J., Shrivastava, M., Donahue, N. M., Gao, Y., Shilling, J. E., Liu, Y., Zaveri, R. A., Gaudet, B., Wang, S.,
 973 Wang, J., Li, Z., and Fan, J.: Formation Process of Particles and Cloud Condensation Nuclei Over the Amazon Rainforest: The
 974 Role of Local and Remote New-Particle Formation, *Geophys. Res. Lett.*, 49, e2022GL100940,
 975 <https://doi.org/10.1029/2022GL100940>, 2022.

976 Zhou, Y., Hakala, S., Yan, C., Gao, Y., Yao, X., Chu, B., Chan, T., Kangasluoma, J., Gani, S., Kontkanen, J., Paasonen, P.,
 977 Liu, Y., Petäjä, T., Kulmala, M., and Dada, L.: Measurement report: New particle formation characteristics at an urban and a
 978 mountain station in northern China, *Atmospheric Chem. Phys.*, 21, 17885–17906, <https://doi.org/10.5194/acp-21-17885-2021>,
 979 2021.

980



981
982 Figure 1. Map of measurement locations included in this study. The number markings indicate the exact locations
983 of the measurements. Created using a template from Canva (www.canva.com)

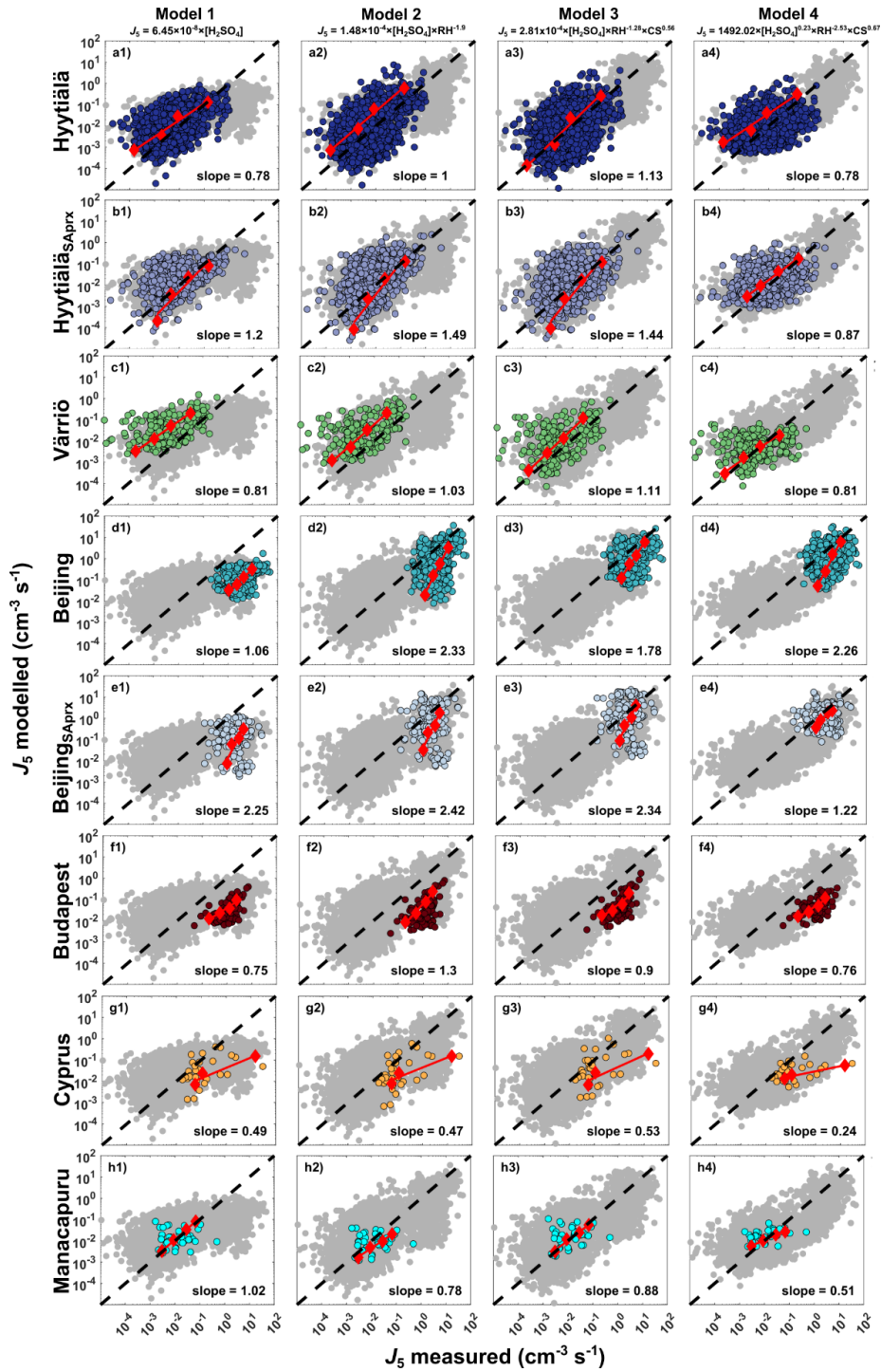


984

985 Figure 2. Modelled and measured J_5 scatterplots in logscale from four models using the testing dataset containing
 986 data from all sites in hourly time resolution. Each color represents the data from one measurement site, including
 987 datasets with H_2SO_4 proxy data from Hyytiälä and Beijing. The straight line showed the robust linear fit between
 988 the logscale modelled and the measure J_5 values, and the dashed line represented the 1:1 line. The correlation
 989 coefficient r , slope of linear fit, and the coefficient of determination R^2 are shown in the title of each subplot.

990

991

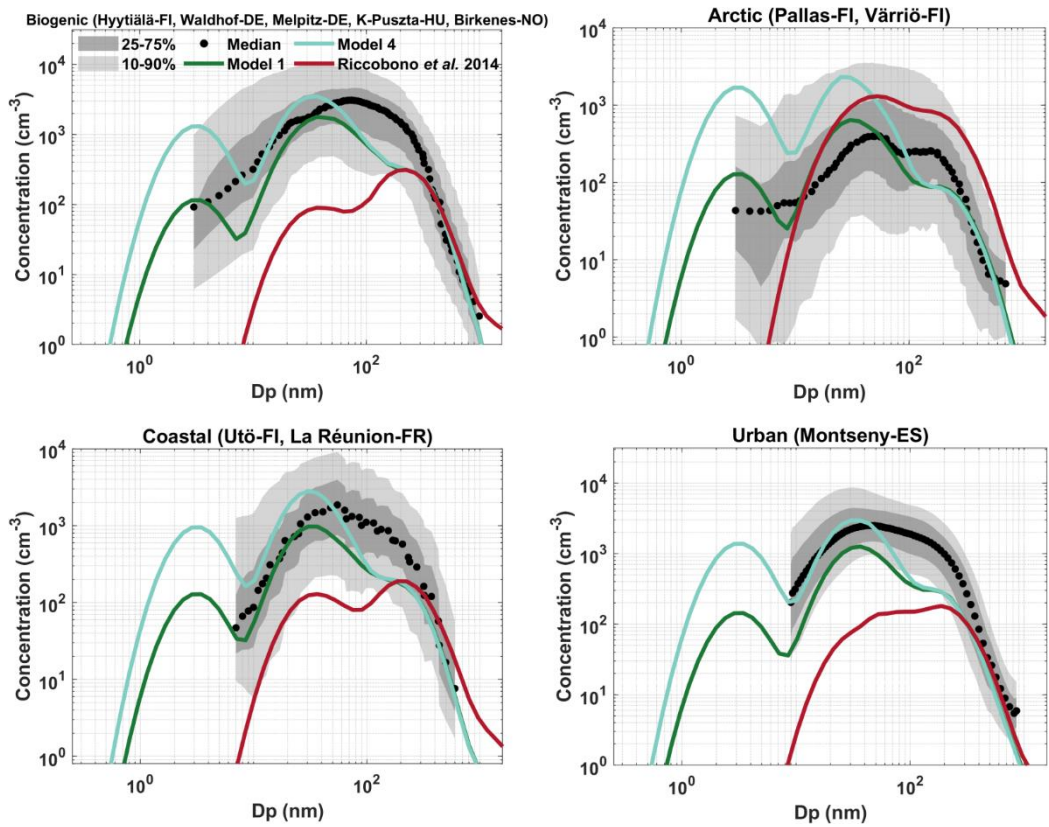


992

993 Figure 3. Modelled and measured J_5 scatterplots in logscale from four models using the testing dataset containing
 994 data from all sites in hourly time resolution. The labels on the left side of the y-axis are the site names. The

995 subscribed label “SAprx” indicates that the input H_2SO_4 concentrations was from H_2SO_4 proxies. The light grey
 996 scatters are all data points from the testing dataset, the colored scatters on top of them indicate the results from the
 997 corresponding measurement site. The red diamonds are the binned daily medians to show the temporal aggregation
 998 of the model performances on daily scale data. Overall, on a daily scale presents excellent performances on model
 999 4 for boreal forest environment (a4, b4 and c4), polluted cities (d4, e4) and organic vapor dominated high humidity
 1000 region (h1-h3). The red solid lines represent the linear fit on the binned hourly medians. The dashed line is the 1:1
 1001 line.

1002

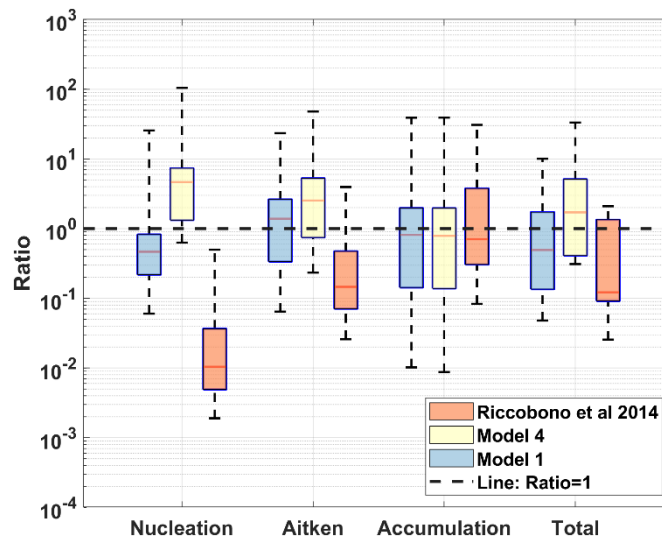


1003
 1004 Figure 4. Environment-specific TM5-MP simulated particle number size distribution from 2018 in annual medians.
 1005 Biogenic sites include rural and rural regional background environments (Hyytiälä, Waldhof, Melpitz, K-Pusztá
 1006 and Birkenes); Coastal sites cover islands on the Baltic Sea and on the Indian Ocean in the southern hemisphere
 1007 close to Madagascar (Utö and La Réunion); Arctic sites are two Finnish sites both situate within the Arctic Circle
 1008 (Pallas and Värriö); Urban site is represented by a Spanish city Montseny.

1009

1010

1011



1012
 1013 Figure 5. Ratio of simulated and measured particle number concentrations from the 14 global sites from TM5-MP
 1014 simulations under three nucleation settings (Riccobono, model 1, and model 4) resulting in three particle modes
 1015 (nucleation, Aitken, accumulation) in 2018 annual medians. The black line represents “ratio = 1” as a reference
 1016 line. The “Total” represents the overall ratio between the simulation and the measurement particle number
 1017 concentrations from all modes.

1018

1019

Table 1. Number of data points from each measurement site. The numbers in column “Total” account for the data points from six-site combined dataset utilized in model training and testing. The training set contains 75% of the total training data points, and 25% for testing set.

Sites	Hyytiälä	Beijing	Värriö	Budapest	Cyprus	Manacapuru	Hyytiälä _{proxy}	Beijing _{proxy}	Total
Training	5003	1342	728	367	140	140	-	-	7720
Testing	1642	501	248	109	34	40	797	164	3535

Table 2. Coefficient values (k_x , k_{RH} , k_{CS} , k_{SA}) retrieved from parameterization using training dataset. The term SSe represents the sum of squared error of each model. The units of k_x ($x = 1, 2, 3, 4$) vary as the functional form of model changes, while k_{RH} , k_{CS} , k_{SA} do not contain units. Since RH is counted using percentage (%), a dimensionless number, the scaling coefficients k0 count mainly the units from H₂SO₄ concentrations and CS. As such, we must ensure that the RH input is in percentage.

Models	Functional forms	k_x	k_{RH}	k_{CS}	k_{SA}	SSe
1	$k_1 \times [H_2SO_4]$	$6.45E-8 \text{ (s}^{-1}\text{)}$				$2.78E+03$
2	$k_2 \times [H_2SO_4] \times RH^{k_{RH}}$	$1.48E-4 \text{ (s}^{-1}\text{)}$	-1.9			$5.16E+03$
3	$k_3 \times [H_2SO_4] \times RH^{k_{RH}} \times CS^{k_{CS}}$	$2.81E-4 \text{ ([s}^{-1}\text{)]}^{0.45}\text{)}$	-1.28	0.56		$5.18E+03$
4	$k_4 \times [H_2SO_4]^{k_{SA}} \times RH^{k_{RH}} \times CS^{k_{CS}}$	$1492.02 \text{ ([cm}^{-3}\text{)]}^{0.78} \times \text{[s}^{-1}\text{)]}^{0.33}\text{)}$	-2.53	0.67	0.23	$3.36E+03$

Table 3. Summary of overall and site-specific correlation coefficients (r) four models using the testing dataset. The numbers in brackets under the site names represent the count for data points.

Slopes and r (robust linear fit), logscale										
	Models	Hyytiälä (1642)	Beijing (501)	Värriö (248)	Budapest (109)	Cyprus (34)	Manacapuru (40)	Hyytiälä _{SA} (797)	Beijing _{SA} (164)	Overall
Slope	1	0.43	0.33	0.32	0.58	0.35	0.04	0.34	0.07	0.30
	2	0.62	0.57	0.40	0.66	0.48	0.15	0.57	0.23	0.58
	3	0.48	0.43	0.32	0.85	0.37	0.18	0.42	0.12	0.64
	4	0.25	0.28	0.12	0.48	0.17	0.24	0.28	0.12	0.62
r	1	0.43	0.30	0.44	0.54	0.42	0.04	0.41	0.004	0.55
	2	0.47	0.32	0.47	0.46	0.49	0.19	0.48	0.07	0.69
	3	0.37	0.30	0.35	0.61	0.38	0.21	0.36	0.02	0.71
	4	0.31	0.22	0.18	0.51	0.37	0.46	0.33	0.09	0.78